5 RESULTS AND DISCUSSIONS

5.1 Antibiotic sensitivity test

An antibiotic susceptibility test determined the bacteria's susceptibility or influence toward various antibiotics. *A. baumannii* was found resistant to piperacillin/tazobactam, cefepime, co-trimoxazole, amikacin, ceftriaxone, gentamicin, cefalexin, ampicillin, and ofloxacin medications, whereas it was susceptible to polymyxin-B, ertapenem, and nitrofurantoin (**Fig. 5.1 and Table 5.1**).

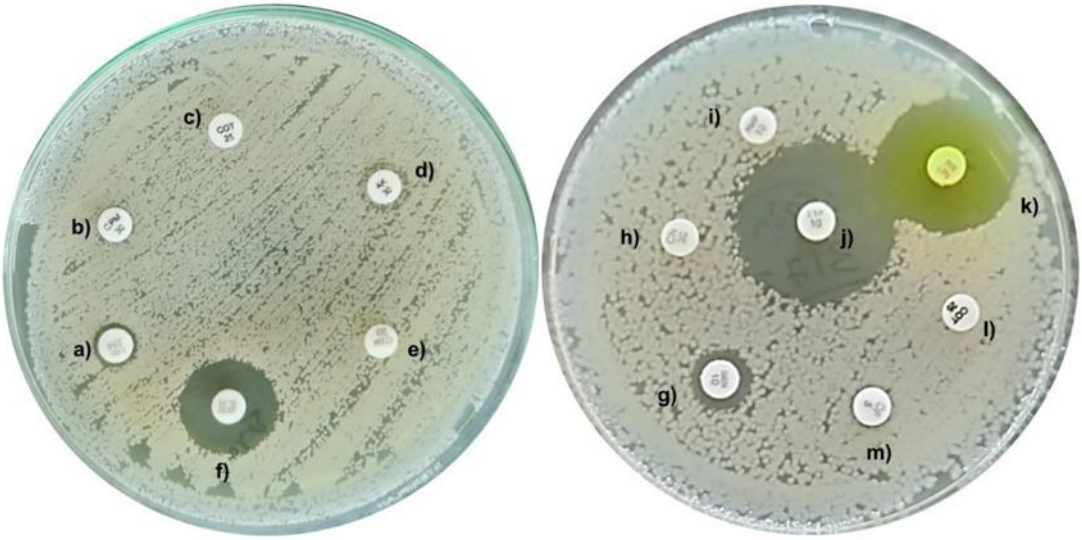

Figure 5.1 Antibiotic sensitivity test of *Acinetobacter baumannii* (BHU/AB/39)

Table 5.1 Antibiotic sensitivity test of *Acinetobacter baumannii* (BHU/AB/39)

S. No	Symbol	Antibiotics	Standard resistant zone diameter (mm)	Result zone diameter (mm) (n=3)	Result
a.	PIT	Piperacillin/ Tazobactam (100/10 mcg)	≤ 17	8±0.00	Resistant
b.	CPM	Cefepime (30mcg)	≤ 14	6±0.00	Resistant
c.	COT	Co–Trimoxazole (25mcg)	≤ 19	6±0.20	Resistant
d.	AK	Amikacin (30mcg)	≤ 14	9±0.00	Resistant

e.	CTR	Ceftriaxone (30mcg)	≤ 13	6±0.20	Resistant
f.	PB	Polymyxin–B (300 units)	≤ 19	16±0.00	Sensitive
g.	GEN	Gentamicin (10mcg)	≤ 12	10±0.00	Resistant
h.	CN	Cefalexin (30 mcg)	≤ 14	6±0.00	Resistant
i.	AMP	Ampicillin (10mcg)	≤ 13	6±0.00	Resistant
j.	ETP	Ertapenem (10mcg)	≤ 18	20±0.00	Sensitive
k.	NIT	Nitrofurantoin (300mcg)	≤ 15	21±0.01	Sensitive
l.	COT	Co–Trimoxazole (25mcg)	≤ 11	6±0.00	Resistant
m.	OF	Ofloxacin (5mcg)	≤ 22	7±0.00	Resistant

As shown in **Fig. 5.2**, *K. pneumoniae* exhibited susceptibility **(Table 5.2)** towards Amikacin while showing resistance against Cefepime, Ertapenem, Imipenem, Oxacillin, Piperacillin/ Tazobactam, Meropenem, Ceftazidime, Ofloxacin, Gentamicin, Cefalexin, and Nitrofurantoin.

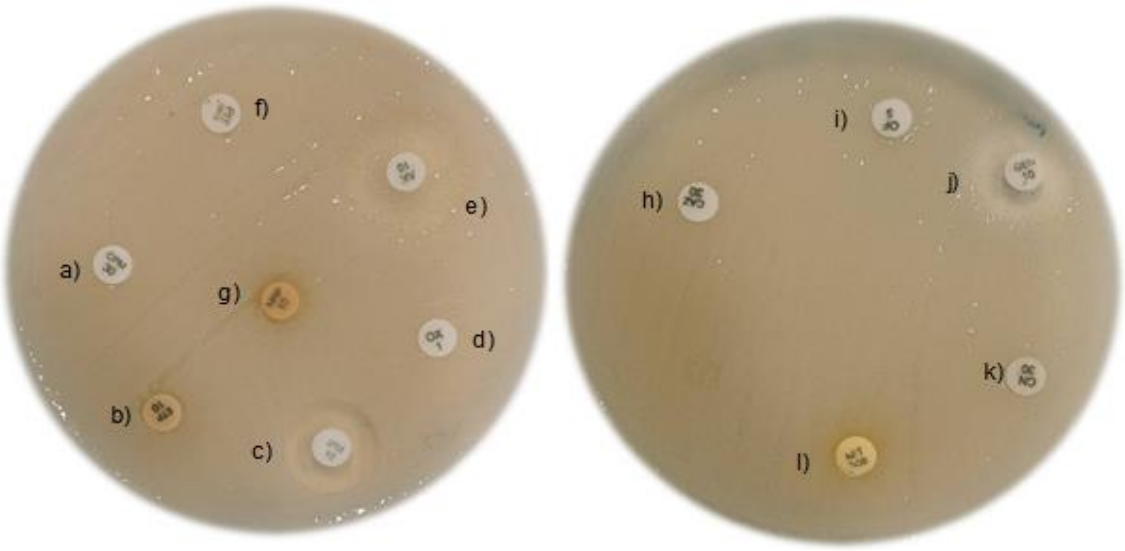

Figure 5.2 Antibiotic sensitivity test of *K. pneumoniae* (BHU/KP/657)

Table 5.2 Antibiotic sensitivity test of *K. pneumoniae*

S. No	Symbol	Antibiotics	Standard resistant zone diameter (mm)	Result zone diameter (mm) (n=3)	Result
a.	CPM	Cefepime (30 mcg)	≥ 18	6±0.00	Resistant
b.	ETP	Ertapenem (10 mcg)	≥ 18	6±0.00	Resistant

c.	IPM	Imipenem IPM (10 mcg)	≥ 19	12±0.20	Resistant
d.	OX	Oxacillin (1 mcg)	≥ 17	6±0.00	Resistant
e.	AK	Amikacin (10 mcg)	≥ 14	16±0.20	Sensitive
f.	PIT	Piperacillin/ Tazobactam (100/10 mcg)	≥ 17	6±0.00	Resistant
g.	MRP	Meropenem (10 mcg)	≥ 19	6±0.00	Resistant
h.	CAZ	Ceftazidime (30 mcg)	≥ 19	6±0.00	Resistant
i.	OF	Ofloxacin (5 mcg)	≥ 12	6±0.00	Resistant
j.	GEN	Gentamicin (10 mcg)	≥ 15	12±0.20	Resistant
k.	CN	Cefalexin (30 mcg)	≥ 14	6±0.00	Resistant
l.	NIT	Nitrofurantoin (300 mcg)	≥ 14	6±0.00	Resistant

Fig. 5.3, exhibits the susceptibility of *S. aureus* **(Table 5.3)** towards co-trimazole, ampicillin+ sulbactam, cefepime, linezolid, clindamycin, amikacin, and vancomycin and resistance against ampicillin, cefotaxime, gentamycin, penicillin, erythromycin, and ciprofloxacin.

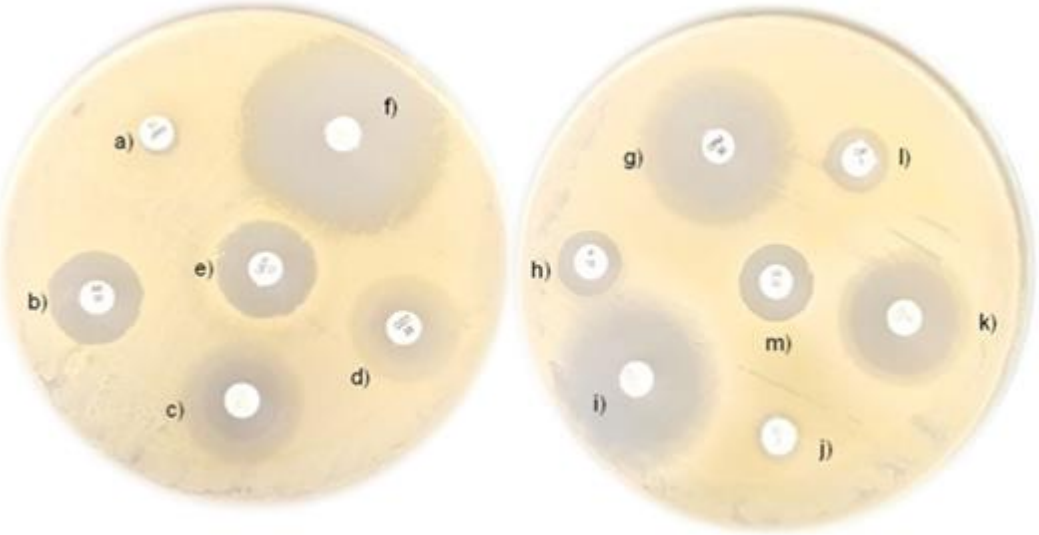

Figure 5.3 Antibiotic sensitivity test of *S. aureus* (BHU/SA/4193)

Table 5.3 Antibiotic sensitivity test of S. aureus

S. No.	Symbol	Antibiotics	Standard resistant zone diameter (mm)	Result zone diameter (mm) (n=3)
a.	AMP	Ampicillin (10 µg)	≤ 28	7±0.12
b.	AK	Amikacin (30 µg)	≤ 16	16±0.32
c.	CTX	Cefotaxime (30 µg)	≤ 23	19±0.28
d.	COT	Clotrimazole (30 µg)	≤ 14	18±0.54
e.	GEN	Gentamycin (10 µg)	≤ 18	17±0.47
f.	A/S	Ampicillin (10 µg) + Sulbactam (10 µg)	≤ 11	38±0.86
g.	CPM	Cefepime (30 µg)	≤ 21	27±0.55
h.	P	Penicillin (10 µg)	≤ 28	12±0.13
i.	LZ	Linezolid (30 µg)	≤ 20	29±047
j.	E	Erythromycin (15 µg)	≤ 18	7±0.02
k.	CD	Clindamycin (2 µg)	≤ 14	21±0.39
l.	CIP	Ciprofloxacin (5 µg)	≤ 15	12±0.25
m.	VA	Vancomycin (30 µg)	≤ 14	15±0.11
	Pure drug	Vancomycin (0.1-5 µg/mL)	≥ 2 µg/ml	1.80±0.12 µg/mL

Similarly, **(Fig. 5.4),** *P. aeruginosa* was observed to be susceptible to the antibiotics **(Table 5.4)** polymyxin B, piperacillin + tazobactam, and colistin (MIC 1.5 µg/ml).

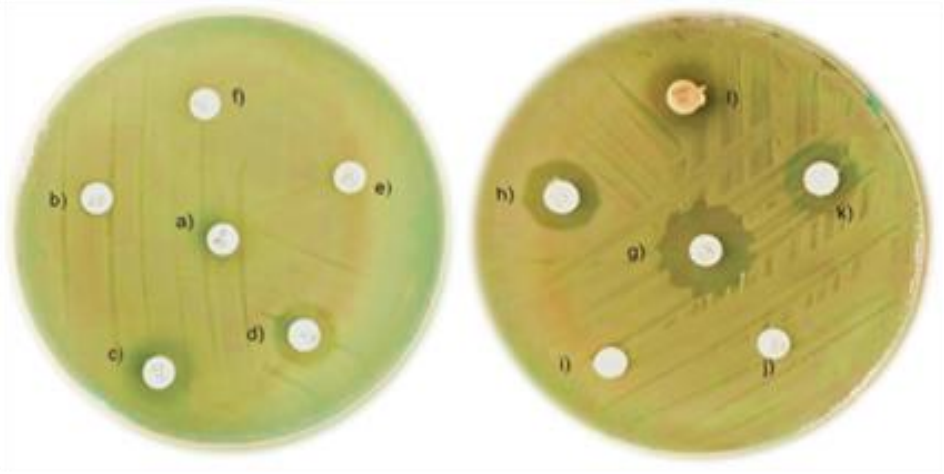

Figure 5.4 Antibiotic sensitivity test of *P. aeruginosa* (BHU/PA/1956)

However, *P. aeruginosa* demonstrated resistance to the antibiotics such as ofloxacin, amikacin, norfloxacin, piperacillin, ceftazidime, gentamycin, aztreonam, cefepime, mipenem, and meropenem antibiotics.

Table 5.4 Antibiotic sensitivity test of *P. aeruginosa*

S. No.	Symbol	Antibiotics	Standard resistant zone diameter (mm)	Result zone diameter (mm) (n=3)
a)	OF	Ofloxacin (5 µg)	≤ 12	7±0.025
b)	AK	Amikacin (10 µg)	≤ 14	6±0.03
c)	NX	Norfloxacin (10 µg)	≤ 12	9±0.17
d)	PI	Piperacillin (100 µg)	≤ 17	11±0.21
e)	CAZ	Ceftazidime (30 µg)	≤ 14	6±0.41
f)	GEN	Gentamycin (10 µg)	≤ 12	6±0.09
g)	PB	Polymyxin B (300 unit)	≤ 11	18±0.19
h)	PIT	Piperacillin + Tazobactam (100 µg/10 µg)	≤ 14	14±0.06
i)	ATM	Aztreonam (30 µg)	≤ 15	6±0.15
j)	CPM	Cefepime (30 µg)	≤ 14	7±0.08
k)	IPM	Imipenem (10 µg)	≤ 15	8±0.33
l)	MRP	Meropenem (10 µg)	≤ 15	8±0.12
	Pure drug	Colistin (0.1-5µg/mL)	≤ 2µg/mL	1.5± 0.73 µg/mL

The obtained data suggested that all bacteria *A. baumannii, K. pneumoniae, S. aureus,* and *P. aeruginosa* bacteria were resistant to multiple (more than three) classes of antibiotics and hence could be considered as MDR strains. MDR *P. aeruginosa-S. aureus* co-infections have been reported to be more dangerous than single infections of either species (Serra *et al.*, 2015). *K. pneumoniae* has been designated as one of the critical priority pathogens by the World Health Organisation and poses a growing

concern to global health due to the rapid increase in both AMR and hypervirulent strains (Lan *et al.,* 2021). According to the analysis conducted by Farhadi *et al.,* 2021, the study examined a total of 100 clinical samples of *K. pneumoniae* strains to determine their AMR patterns. The findings revealed that 58% of the strains exhibited multidrug resistance (MDR), while 32% displayed extensively drug-resistant (XDR) characteristics. The study revealed that 93% of the *K. pneumoniae* bacteria exhibited a significantly higher resistance rate toward the ampicillin/sulbactam antibiotic (Farhadi *et al.,* 2021). Isolated bacteria (*A. baumannii, K. pneumoniae, S. aureus,* and *P. aeruginosa*) are the ideal choice for the experiment because of multidrug resistance characteristics and the incredible potential of forming biofilms that are difficult to eradicate.

5.2 Bacteriophage isolation, amplification, and purification

The Bacteriophage (BP) against the multidrug-resistant bacteria *A. baumannii, K. pneumoniae, S. aureus, and P. aeruginosa* were successfully isolated and named as BPABΦ1, BPKPΦ1, BPSAΦ1, and BPPAΦ1 respectively. Also, BPs were amplified in higher titer (~10^{12} pfu/mL) and purified below 0.5EU/mL of endotoxin level.

5.3 Bacteriophage characterization

5.3.1 Plaque assay

The plaque assay was focused on growing isolated plaques of phages particles within a lawn of host bacteria, and DLAO quantified the grown BPs. The resultant plaque shows a visible clear, round shape, neat border with an average size of 6.68 ± 0.94 mm for *A. baumannii*, 6.53±0.86 mm for *K. pneumoniae* 1.03±0.12 mm for *S. aureus* and 4.8±0.45 mm for *P. aeruginosa* **(Fig. 5.5)**. Also, all phages showed narrow-lytic range. Researchers reported, tiny, pinpoint plaques of phage (2 ± 0.23 mm) isolated against *S.*

aureus and small, clear, round plaques of phage against *P. aeruginosa* with a diameter of approximately 2 ± 0.23 mm (Kaur *et al.*, 2021; Sharma *et al.*, 2021; Teng *et al.*, 2022). Additionally, it has been stated that Lytic BPs exhibit clear plaques, whereas lysogenic phages display turbid or bulls-eye plaques (Ramesh *et al.*, 2019). However, only molecular genome sequencing will assure the existence of lytic and lysogenic phage (Gudlavalleti *et al.*, 2020).

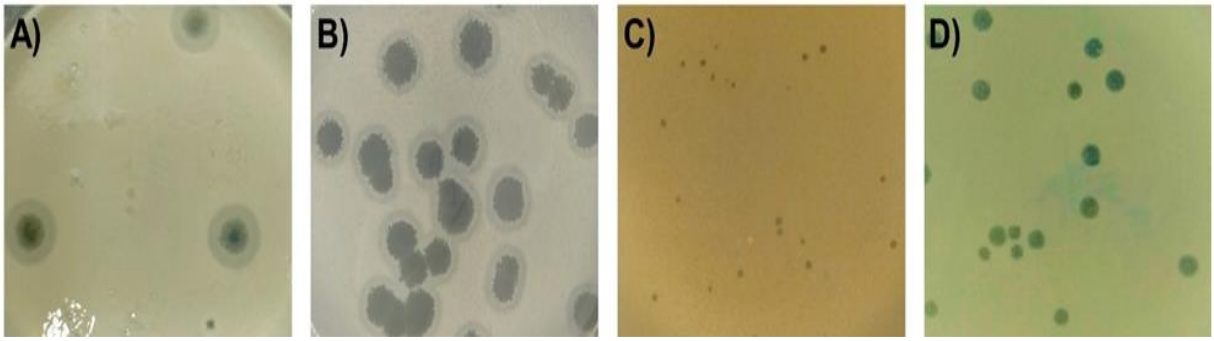

Figure 5.5 Plaques of bacteriophage A) BPABΦ1 phage against *A. baumannii*, B) BPKPΦ1 phage against *K. pneumoniae*, C) BPSAΦ1 phage against *S. aureus*, and D) BPPAΦ1 phage against *P. aeruginosa*

5.3.2 Morphological evaluation of bacteriophage

Based on morphology analysis of BPs found that BPABΦ1 (**Fig. 5.6a**) showed a hexagonal head about 85.93 ± 3.93 nm in diameter but without a neck and a tail, which categorized them under the *Corticoviridae* family (King *et al.*, 2012). The TEM images of the BPKPΦ1 (**Fig. 5.6b**) showed that BPKPΦ1 has an icosahedral capsid (head) of 92.15±2.09 nm (in diameter), a tail of 355.17±2.67 nm (in length), and flexible, non-contractile tail fibers of 447.32±0.82 nm (in length). Furthermore, the morphological imaging of the BPs by TEM showed that BPSAΦ1**(Fig. 5.6c)**. has an icosahedral head capsid with a diameter of 88.9±9 nm, tail (115.2±3 nm long), and tail fibers, which is flexible with a full length of 201.1±1 nm. Similarly, BPPAΦ1 (**Fig. 5.6d**) TEM images showed an icosahedral head capsid (143.7±1.05 nm), long thin tail (193.7±1.14 nm), having thin tail fibers and flexible with full length up 337.3± 1.1 nm. According to the

latest guidelines set forth by the International Committee on Taxonomy of Viruses (ICTV), BPSAΦ1 and BPPAΦ1 have been assigned as members of the *Caudoviricetes* class.

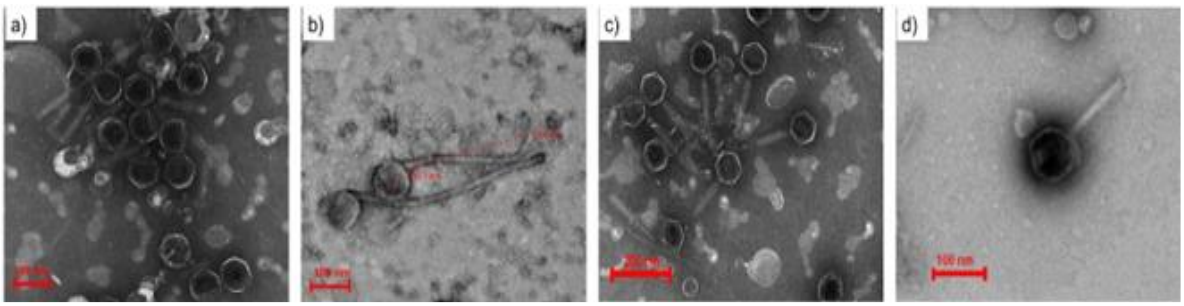

Figure 5.6 Morphology of bacteriophage analysed by TEM A) BPABΦ1 B) BPKPΦ1 C) BPSAΦ1and D) BPPAΦ1

5.3.3 Singular step growth curve

To determine the proliferation rate of BPs in a host cell, the latent period, and the burst size per infected bacterial cell, the singular-step growth curves of study for BPs were performed. The obtained data were analyzed, and triphasic curves were plotted **(Fig.5.7),** it was observed that the BPABΦ1, BPKPΦ1, BPSAΦ1, and BPPAΦ1 phages had a latent period of 25, 20, 25, and 15 min, respectively.

In terms of burst size BPABΦ1, BPKPΦ1, BPSAΦ1, and BPPAΦ1 exhibit 102, 129, 75, and 112 PFUs per infected host cell respectively. The burst size and latency period are essential factors to consider in the context of bacteriophages' potential therapeutic applications. Han *et al.* (2013) found that Staphylococcus phage SAH-1 had a 20min latent period and 100 PFU/cell burst size (Han *et al.*, 2013). The same factors were also observed for the phages SA (30 min, 1000 phages) and MSA6 (15 min, 23 PFU/cell) (Hamza *et al.*, 2016; Titze *et al.*, 2020). The higher burst size and shorter latent duration are thought to be advantageous, although there are situations, such as

when the host bacterial cell density is low when a more prolonged latent period is required (Mohammadian *et al.*, 2022).

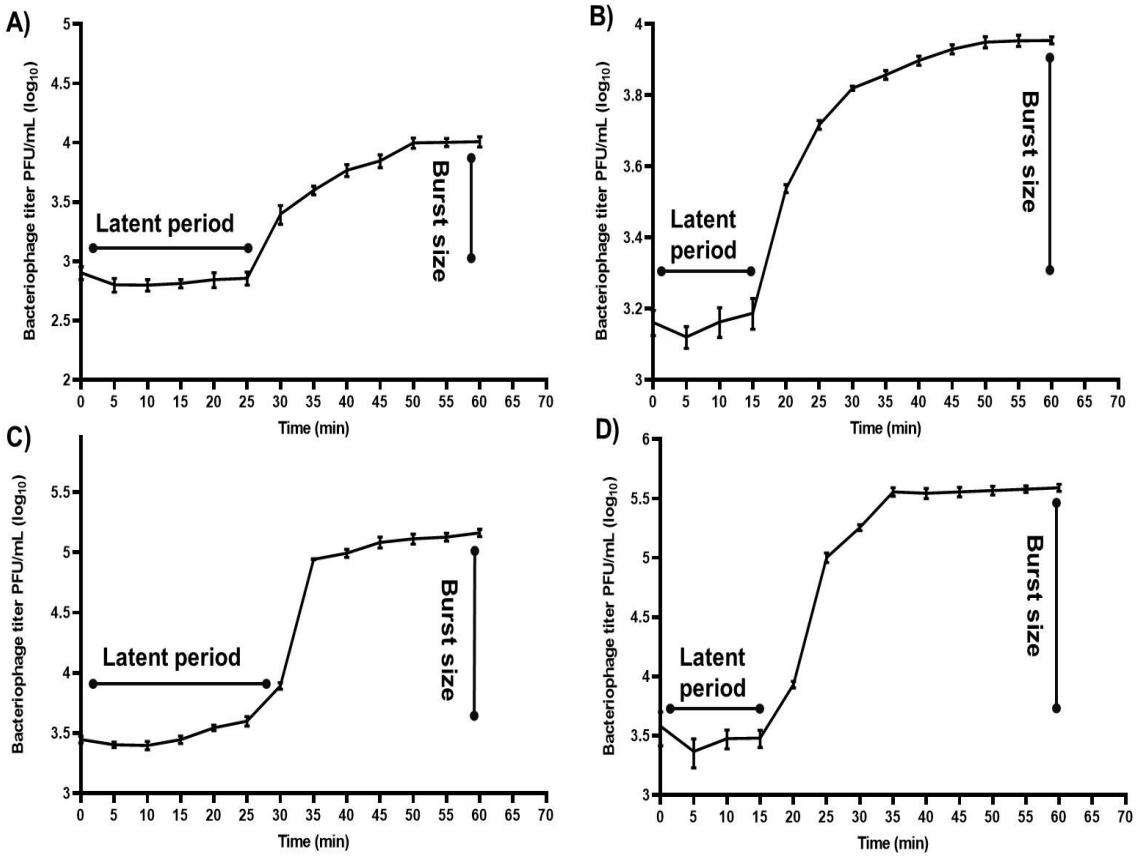

Figure 5.7 One step growth curve of bacteriophage A) BPABΦ1 B) BPKPΦ1 C) BPSAΦ1 and D) BPPAΦ1

5.3.4 pH, temperature, and U.V. stability studies of bacteriophages

This study was carried out to determine the optimal pH and temperature for the development of BP formulations (**Fig 5.8)**. When phages were tested to various pH conditions, it was discovered that the PFU of BPABΦ1 and BPPAΦ1 phages had greater titers in the pH range of 6.8 to 7.4, whereas BPKPΦ1and BPSAΦ1had higher stable titers in the pH range of 6.8 to 8.5 **(Fig. 5.8(A)-(C)),** but no active phage was found at pH 1.5, pH 9. Further, in the case of temperature stability, all phages are stable below 50°C, but degraded above 60°C **(Fig. 5.8(D) -(F))**.

Also, within 5 min of UV exposure, the half titer of all phages gets decreased and eventually got completely killed within 10 min; hence UV sterilization was not found to

be suitable for BP formulation. The formulation can be prepared within pH 6.8-7.4 at a temperature below 40℃.

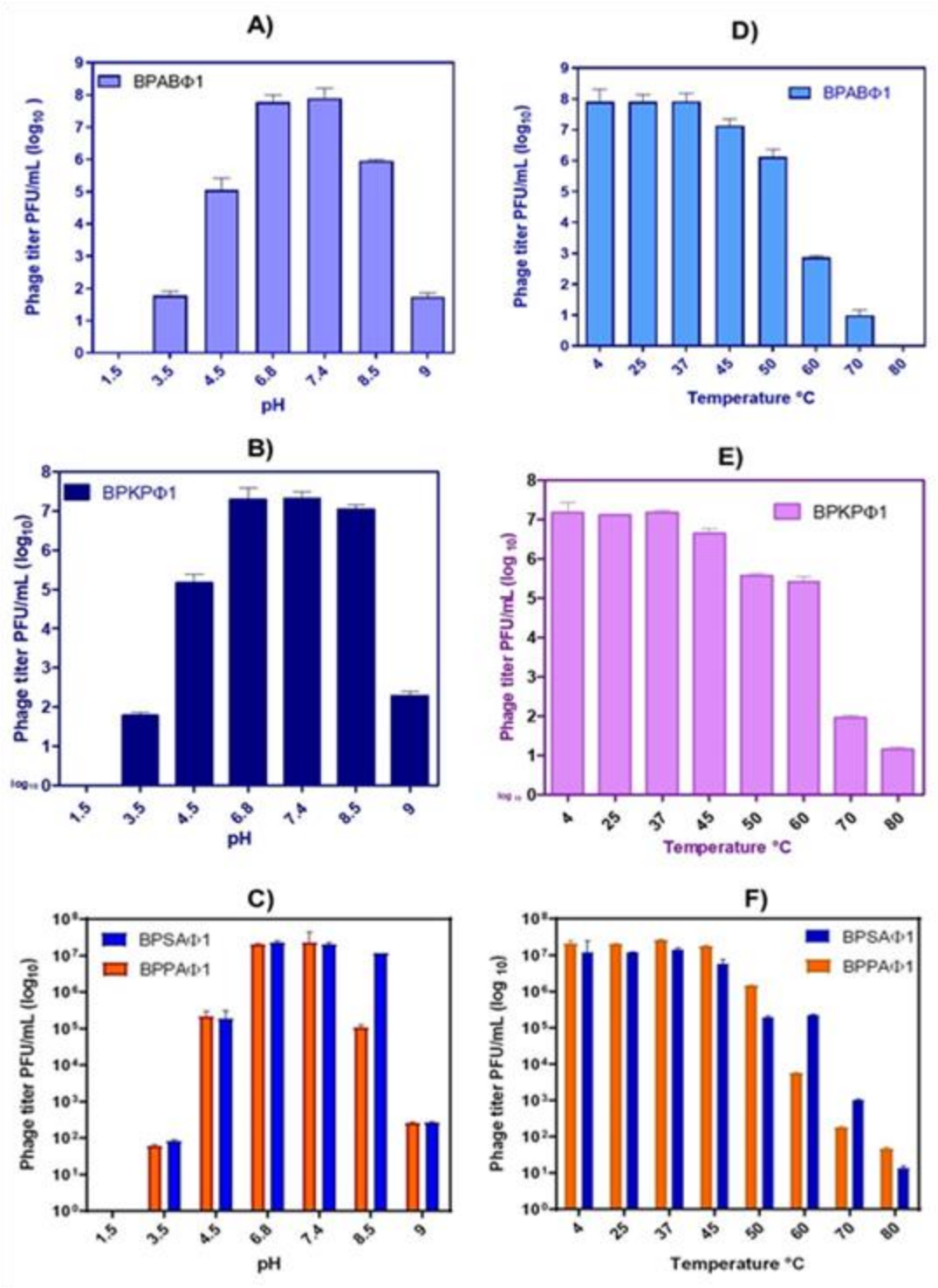

Figure 5.8 pH stability study of bacteriophages Where, A) BPABΦ1 titers, B) BPKPΦ1 titers, C) BPSAΦ1 titers, and D) BPPAΦ1 titers. Stability study of bacteriophages where D) BPABΦ1 titers, E) BPKPΦ1 titers, F) BPSAΦ1 titers, and G) BPPAΦ1 titer at different temperatures

Previous studies have also reported similar findings regarding the stability of phages within a pH range of 5-9 and a temperature range of 4-60°C (Ahmadi *et al.*, 2017; Jończyk *et al.*, 2011b; Khawaja *et al.*, 2016). Nevertheless, the stability of phages exhibits variation in accordance with their diversity (Jończyk *et al.*, 2011b). A similar study conducted by Feng *et al.*, 2003 investigated the impact of temperature and pH on the viability of coliphages (MS2 and Qβ) in both wastewater and water. The phages exhibited the lowest inactivation rate when subjected to pH levels ranging from 6-8 and temperature ranges between 5°C-35°C (Feng *et al.*, 2003). Furthermore, several studies have shown that pH values below 4 and above 9, as well as temperatures above 40°C, generally restrict phage activity and viability (Jończyk *et al.*, 2011b; Pallavi *et al.*, 2021; Pradeep *et al.*, 2022). The highly acidic pH and extreme temperature cause protein denaturation and destruction to the physical structure of the phage, compromising its ability to regulate biologically (Ramirez *et al.*, 2018). Therefore, microencapsulation could protect bacteriophages from hostile environmental conditions.

5.3.5 Hemocompatibility assay of bacteriophages

The hemolysis study suggested the hemocompatibility nature of the BPs. According to national biological safety guidelines, if the rate of hemolysis is less than 2%, the BPs are classified as non-hemolytic. The hemolysis rates of BPKPΦ1, BPSAΦ1 and BPPAΦ1 phages were found to be 0.83±0.46%, 0.55±0.19%, 1.06±0.08%, and 0.91±0.014% respectively. Additionally, the negative control (Normal saline) demonstrated hemocompatibility while the positive control (TritonX100) fully ruptured the RBCs. The hemocompatibility study demonstrated that BPs are hemocompatible and nonhemolytic to RBCs **(Fig. 5.9).** However, prior research found that whole blood completely, partially, or no inhibition of phage activity against bacteria *in vitro* (Congress, 1939; Podlacha *et al.*, 2021).

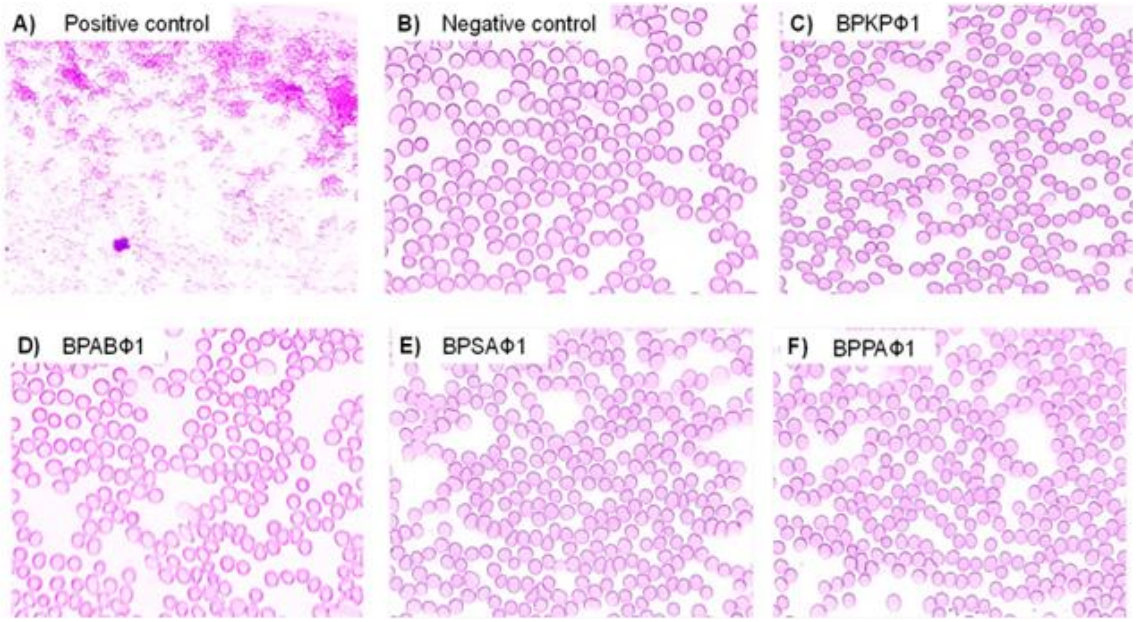

Figure 5.9 Represents the images of the hemocompatibility study (40X resolution), where A) positive control group (TritonX100), B) negative control group (normal saline), C) BPABΦ1, D) BPKPΦ1, E) BPSAΦ1, and F) BPPAΦ1.

5.4 Formulations development and characterizations

BPs and excipients (chitosan, trehalose, sodium TPP, glycerol, and Sepineo^{TM} P 600) compatibility study was performed by incubating the BPs separately in the presence of excipients for 24 h at 37°C. It was observed that there was no significant decrease in the titer of BP. This observation strongly suggests that the selected excipients used in the formulation are highly compatible with BP. The absence of any decline in the titer indicates that the excipients do not negatively impact the stability or viability of the BPs.

The chitosan microparticles were developed by the ionic gelation method in the presence of sodium TPP. BPs were dispersed in the polymeric solution of the chitosan and the gradual addition of the sodium TPP under magnetic stirring triggered the ionic crosslinking of the chitosan amine group (positively charged) and phosphate group (negatively charged) of the sodium TPP. The dispersed BPs get entrapped inside the polymeric matrix of the chitosan microparticles. We have prepared the 4 microparticles (BPABΦ1-CHMPs, BPKPΦ1-CHMPs, BPSAΦ1-CHMPs, BPPAΦ1-CHMPs) specific

for single bacterial wound infection (*A. baumannii, K. pneumoniae, S. aureus and P. aeruginosa*). Additionally, One MBP-CHMPs (co-entrapment of BPSAΦ1- BPPAΦ1) and MBP-CHMPs-gel for treatment of polybacterial infections (*S. aureus and P. aeruginosa*). Moreover, bacteriophage microencapsulation using chitosan and other polymers has been reported in several studies against numerous infectious diseases (Ilomuanya *et al.*, 2022; Kim *et al.*, 2015; Ma *et al.*, 2008b)

5.4.1 Particle size, polydispersity, zeta potential, and entrapment efficiency

Before the incorporation of microparticles in gel optimization based on Particle size, polydispersity, zeta potential, and entrapment efficiency were carried out (**Table 5.5**). Based on the higher percentage of the bacteriophage's entrapment as well as its suitability for use in both moderate and severe deeper wound infections for local effect, the bacteriophage particle size was optimized. Microparticles are generally easier to prepare, handle, and characterize. Their larger size allows for the controlled release of bacteriophage over an extended period, providing sustained therapeutic effects. Microparticles are generally more stable than nanoparticles. The size range (1-2 µm) was decided to achieve for having maximum retention at the site of action for better therapeutic efficacy (Daly *et al.*, 2020; Hong *et al.*, 2017).

Table 5.5 Particle size, polydispersity index, zeta potential, and entrapment efficiency of different formulations

	Particle size (µm)	**Polydispersity**	**Zeta potential (mV)**	**EE(%)**
Blank CHMPs	1.04±0.83	0.30±0.50	20.20±0.03	-
BPABΦ1-CHMPs	1.29±0.78	0.40±0.17	26.41±0.61	91.30±1.94
BPKPΦ1-CHMPs	1.96±0.53	0.28±0.45	32.16±0.40	82.44±1.31
BPSAΦ1-CHMPs	1.19±0.12	0.45±0.41	26.37±0.20	88.68±1.17

BPPAΦ1-CHMPs	1.42±0.21	0.19±0.30	29.04±0.36	82.54±1.22
MBP-CHMPs	2.04±0.28	0.43±0.53	32.11±0.59	78.56±1.03 (BPSAΦ1) and 69.52±0.84 (BPPAΦ1)

Blank CHMPs: Blank chitosan microparticles
BPABΦ1-CHMPs: Bacteriophage against *A. baumannii* chitosan microparticles
BPKPΦ1-CHMPs: Bacteriophage against *K. pneumoniae* chitosan microparticles
BPSAΦ1-CHMPs: Bacteriophage against *S. aureus* chitosan microparticles
BPPAΦ1-CHMPs: Bacteriophage against *P. aeruginosa* chitosan microparticles
MBP-CHMPs: Mixed bacteriophage chitosan microparticles

5.4.2 Gel characterization

The prepared MPs were incorporated into the Sepineo^{TM} P 600 gel. Microparticle laden gel named as BPABΦ1-CHMPs-gel, BPKPΦ1-CHMPs-gel, BPSAΦ1-CHMPs-gel, BPPAΦ1-CHMP gel, and MBP-CHMPs-gel. Based on the organoleptic evaluation of gels, it was found that all gels had characteristics such as odorless, homogeneous, and semi-transparent. In addition, in terms of spreadability, prepared gel indicates that it can be easily spread across a larger area with less pressure, and it creates a layer that is thin on the applied surface. Furthermore, viscosity of BPABΦ1-CHMPs-gel, BPKPΦ1-CHMPs-gel, BPSAΦ1-CHMPs-gel, BPPAΦ1-CHMPs-gel, and MBP-CHMPs-gel was found to be 3137.51±33.45, 2914.03±46.13, 3298.24±0.05, 3370.18±0.63, and 3384.6±0.88 cP, respectively.

5.4.3 Morphological evaluation of microparticles and gel

Scanning electron microscopy (SEM) was employed to analyze the surface morphology of the BPABΦ1-CHMPs and BPKPΦ1-CHMPs. The BPKPΦ1-CHMPs exhibited a uniform structure and possessed a semi-spherical structure, as shown in (**Fig. 5.10A and B).** Furthermore, the morphology of the BPABΦ1-CHMPs gel and BPKPΦ1-CHMPs gel exhibited characteristics resembling an intricate network composed of non-uniform fibers (**Fig. 5.10C and D).**

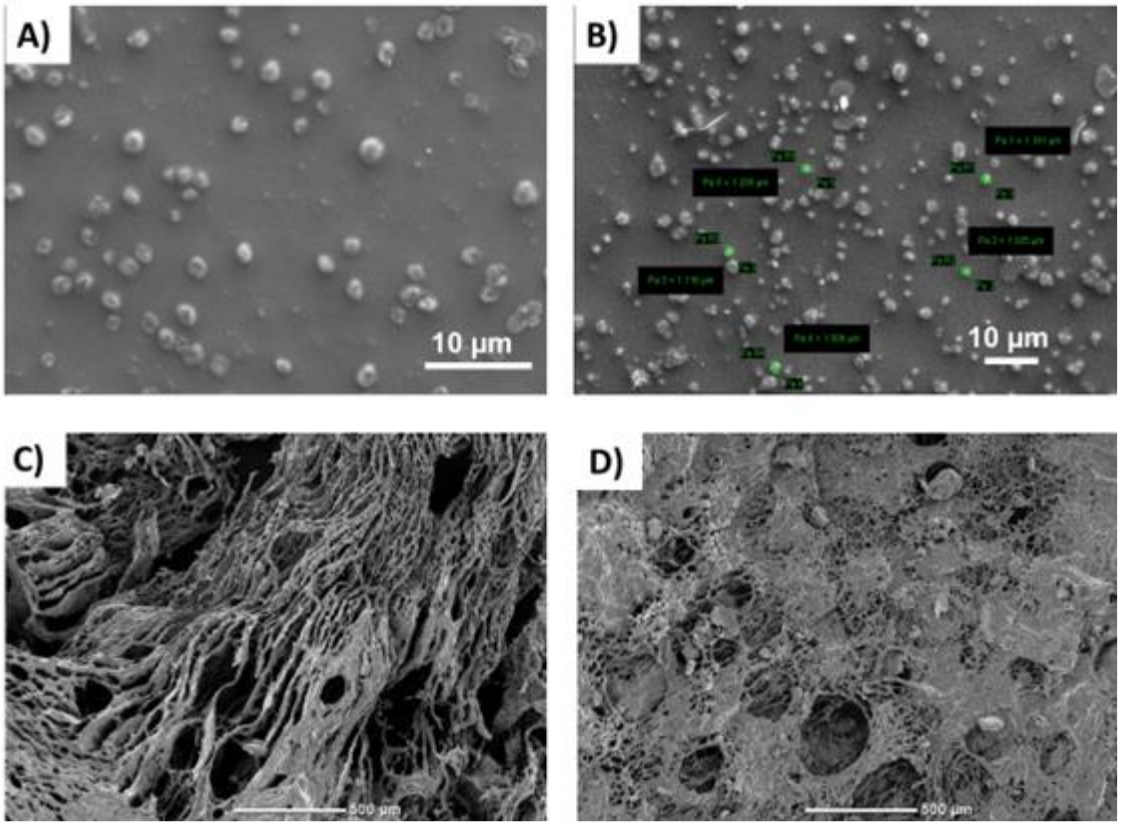

Figure 5.10 Morphological evaluation of bacteriophage formulations by Scanning electron microscopy where: A) SEM image of BPABΦ1-CHMPs, and B) SEM image of BPKPΦ1-CHMPs C) SEM image of BPABΦ1-CHMPs laden gel and D) SEM image of BPKPΦ1-CHMPs laden gel.

Further, formulated MPs **(Fig. 5.11A, B, C)** were also observed to be homogeneous with somewhat spherical-shaped large clusters. Interwoven network of irregular fibers was observed in the BPSAΦ1-CHMPs-gel, BPPAΦ1-CHMPs-gel, and MBP-CHMPs-gel **(Fig. 5.10 D, E, and F)** where chitosan microparticles are embedded. Martins *et al*., 2012 reported similar observations of irregularly shaped large clusters in chitosan/tripolyphosphate microparticles (Martins *et al.*, 2012). However, the type, quantity, and formulation procedure as well as the solvent environment all affect the shape of chitosan microparticles (Sreekumar *et al.*, 2018).

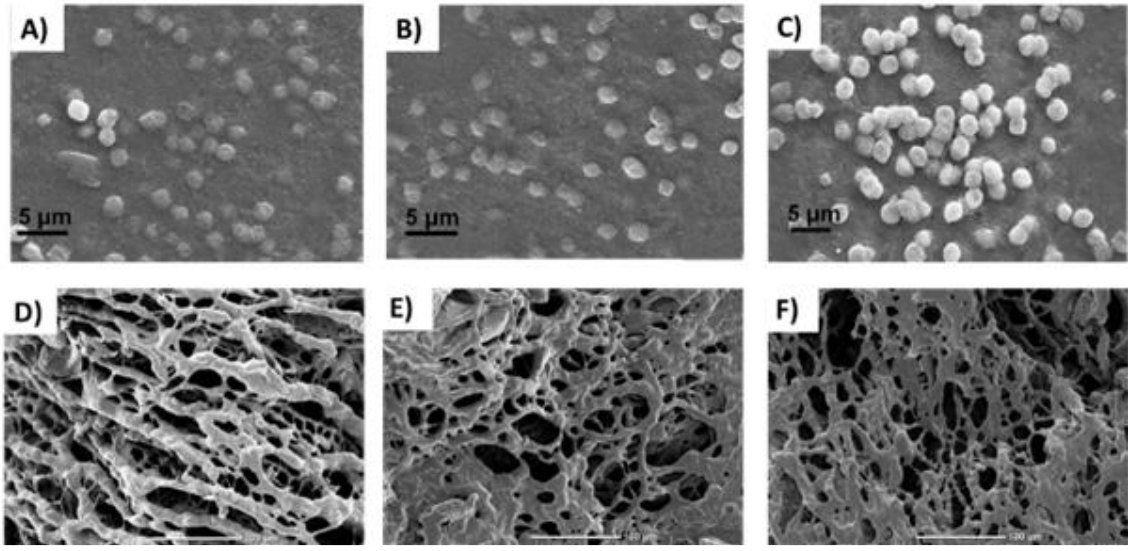

Figure 5.11 Morphological examination and BP release study of the microparticles and gel formulation. Scanning electron microscopy images of A) BPSAΦ1-CHMPs, B) BPPAΦ1-CHMPs, C) MBP-CHMPs, D) BPSAΦ1-CHMPs laden gel, E) BPPAΦ1-CHMPs laden gel, and F) MBP-CHMPs loaded gel.

5.4.4 *In vitro* release study of bacteriophage

In vitro release studies were conducted to determine the availability of bacteriophage at the wound site from microparticle and gel formulations. From the release study, it was found that more than 70% of all phages are released within 30 min, and all of them are completely released in 60 min from phage suspension. From the study, it was observed that 98.34±2.15 and 89.09±2.85 % BPABΦ1 were released from BPABΦ1-CHMPs and BPABΦ1-CHMPs-gel respectively **(Fig. 5.12A**) and 94.81±1.34 and 78.55±2.95 % BPKPΦ1 were released from BPKPΦ1-CHMPs and BPKPΦ1-CHMPs-gel respectively **(Fig. 5.12B**) after 12h. Similarly, BPSAΦ1 and BPPAΦ1 released 94.81±3.71, 91.73±2.53, 79.55±1.96, and 73.12±1.48 % from BPSAΦ1-CHMPs, BPPAΦ1-CHMPs, BPSAΦ1-CHMPs-gel and BPPAΦ1-CHMPs-gel respectively in 12 h **(Fig 5.12C)**. Furthermore, BPSAΦ1 and BPPAΦ1 release from MBP-CHMPs was 94.00±2.16 and 96.16±1.30 % in 12 h.

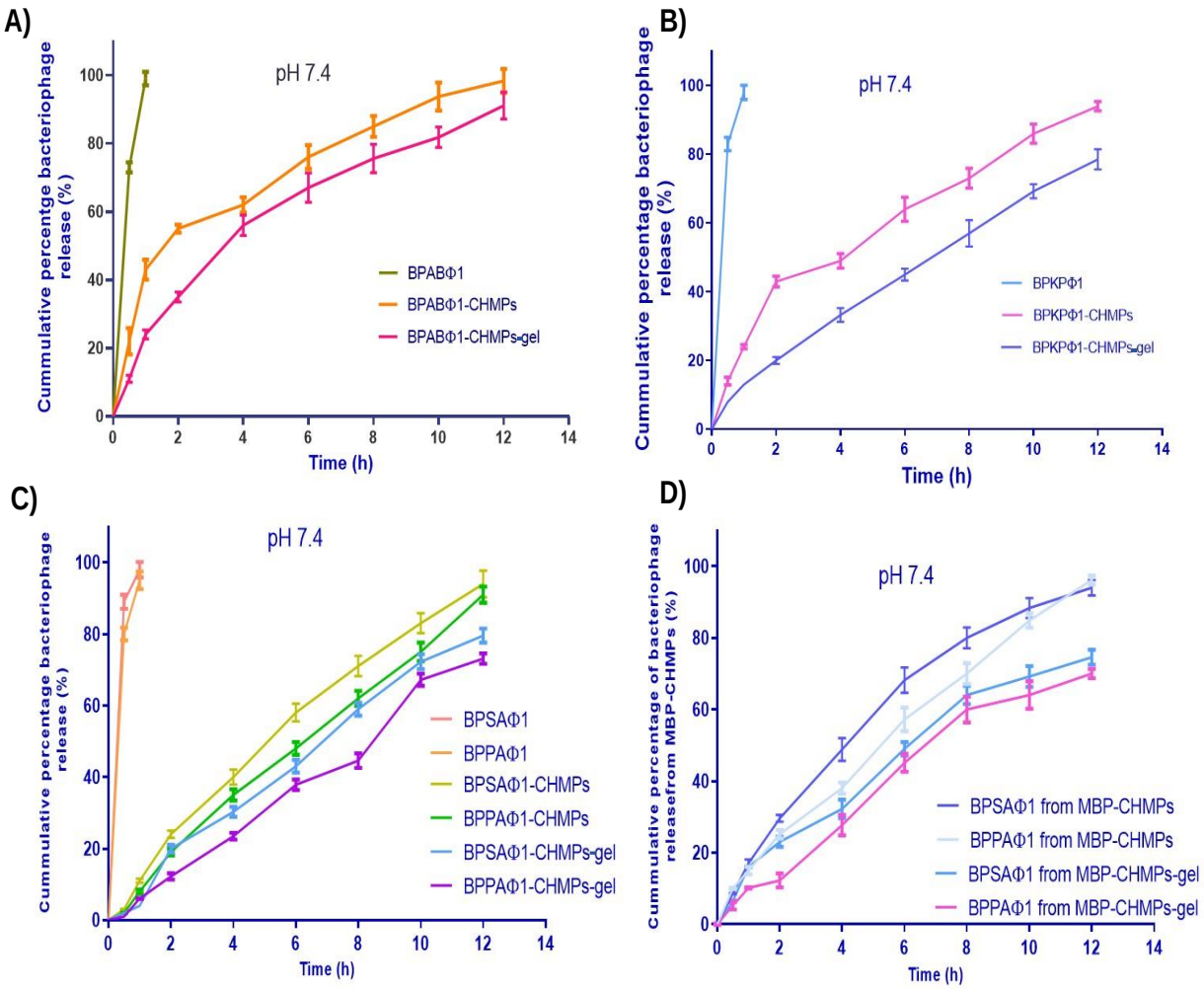

Figure 5.12 In vitro release of the BP from A) free BPABΦ1, BPABΦ1-CHMPs, BPABΦ1-CHMPs, BPSAΦ1-CHMPs gel, B) free BPKPΦ1, BPKPΦ1-CHMPs, BPKPΦ1-CHMPs, BPSAΦ1-CHMPs gel, C) free BPs (BPSAΦ1 and BPPAΦ1), BPSAΦ1-CHMPs, BPPAΦ1-CHMPs, BPSAΦ1-CHMPs gel & BPPAΦ1-CHMPs gel and D) BPs release profile from MBP-CHMPs and MBP-CHMPs laden gel at pH 7.4.

Besides that, the gel effect on BP release (BPSAΦ1 and BPPAΦ1) from MBP-CHMPs-gel was investigated and observed that 74.55±2.06 and 70.30±1.27 % of BPSAΦ1 and BPPAΦ1 were released in 12 h, respectively **(Fig 5.12D).** Hence, the obtained data suggested that the incorporation of the MPs in the gel further sustained the BPs release and could produce an antibacterial effect for a longer period.

Similar findings were observed in a study conducted by Jamaledin *et al.*, 2023, the authors developed microencapsulated BPs in poly (lactic-co-glycolic acid) using a double emulsification approach. A sustained release phenomenon was observed in the

formulations of bacteriophage-loaded microparticles (MPs), characterized by an initial rapid release followed by a gradual and prolonged release (Jamaledin *et al.*, 2023). Likewise, Yongsheng *et al.*, 2012 formulated phage-loaded microparticles to combat the cystic fibrosis-causing S. aureus. The release profile of phage K, when loaded onto the microparticles, exhibited an initial burst release of the phage, which was subsequently followed by sustained release over 12 hours (Kalelkar *et al.*, 2022).

5.5 Antibacterial study

5.5.1 Minimum inhibitory concentration & minimum bactericidal concentration

The quantitative antibacterial activity of formulation was performed, where MIC values of BPABΦ1, Blank CHMPs, and BPABΦ1-CHMPs were found to be $5.6x10^6$ PFU/mL, 480±3.46 µg/mL, 200.0±2.66 µg/mL, respectively, after 24 h of incubation. Additionally, the MBCs values of BPABΦ1, Blank CHMPs, and BPABΦ1-CHMPs formulations were found to be $1.9x10^8$ PFU/mL, 710±2.03 µg/mL, and 250.0±3.68 µg/mL, respectively. Further, the minimum inhibitory concentration (MIC) values for BPKPΦ1, Blank CHMPs, and BPKPΦ1-CHMPs were determined to be $1.8x10^7$ PFU/mL, 450±2.04 µg/mL, and 190±1.48 µg/mL, respectively. Furthermore, the minimum bactericidal concentrations (MBCs) of BPKPΦ1, Blank CHMPs, and BPKPΦ1-CHMPs formulations were determined to be $3x10^8$ PFU/mL, 485±1.64 µg/mL, and 205±2.55 µg/mL, respectively. The MIC values of BPSAΦ1-CHMPs, BPPAΦ1-CHMPs, and MP-CHMPs were found to be 150±2.03, 170±1.08, and 160±1.81 µg/µL, respectively, after 24 h of incubation**.** Additionally, MBCs of BPSAΦ1-CHMPs, BPPAΦ1-CHMPs, and MP-CHMPs were found to be 180±2.01, 185±1.09, and 175±1.05 µg/µL, respectively. The findings revealed no synergistic or antagonistic interaction between BPs (BPSAΦ1 and BPPAΦ1).

Further, both BPSAΦ1/BPPAΦ1 loaded microparticles (MBP-CHMPs) MIC against a mixture of *S. aureus* and *P. aeruginosa* was found to be 160±1.81 µg/µL. This indicates that BPSAΦ1-CHMPs and BPPAΦ1-CHMPs formulations are independently active against respective bacteria. When MBP-CHMPs evaluated against showed intermediate activity (160±1.81 µg/µL), which is higher than BPSAΦ1-CHMPs and lower than BPPAΦ1-CHMPs. The study conducted by Luo *et al.*, 2022 assessed the MIC of phage YC#06, antibiotic, and their combination against *A. baumannii* bacteria. It has been found that the MIC of antibiotics decreased when combined with phages due to the synergistic effect (Luo *et al.*, 2022). Although, treating poly bacterial infections is more difficult and challenging than treating infections caused by a single bacterial infection (Short *et al.*, 2014).

5.5.2 Antibiofilm assay

The biofilm formation over burn wounds leads to the failure of standard burn treatment. In this context, it was revealed that the treatment that can eradicate Biofilm is efficient against burn wounds**.** Used bacterial strain *A. baumannii, K. pneumoniae, S. aureus, P. aeruginosa, poly bacterial biofilm* (*S. aureus*, and *P. aeruginosa*) formed strong biofilm (>4×OD of control growth media). Further, from the study, it was observed that BPABΦ1-CHMPs (88.69±3.11 %), and BPABΦ1-CHMPs (94.46±2.19 %), showed a significant (P<0.05) biofilm eradication; however, only 21.57±0.66 % of biofilm eradication was observed in case of blank CHMPs following the 24 h treatment, which was found to be significant, compared to BPABΦ1, and BPABΦ1-CHMPs**.** Furthermore, significant *K. pneumoniae* biofilm eradication rates for BPKPΦ1 and BPKPΦ1-CHMPs, with values of 60.43±1.77 and 79.23±2.08 %, respectively (P<0.05); however, only 25.94±0.91% of biofilm eradication was observed in case of blank

CHMPs following the 24 h treatment, which was found to be significant, compared to BPKPΦ1, and BPKPΦ1-CHMPs**.**

Further, obtained results depicted that BPSAΦ1-CHMPs, BPPAΦ1-CHMPs, and MBP-CHMPs had significant (P<0.05) biofilm eradication with 88.43±1.04, 81.31±0.53, and 85.68±0.28%, respectively. In contrast, after 24 hours of treatment, the blank CHMP-treated group showed only 10.01±0.3% eradication of *S. aureus* biofilm, 7.41± 0.38% eradication of *P. aeruginosa* biofilm, and 6.62±0.94% eradication of mixed biofilm, which is insignificant in compare with the control biofilm.

Bacteriophages prohibit biofilm development by a) inhibiting cell-to-cell signaling (quorum sensing), b) penetrating mature biofilms, c) producing EPS degrading enzymes, endolysins, hydrolase, and polysaccharide depolymerase, d) lysing the bacterial cell, and e) host specific lytic activity (Amankwah *et al.*, 2021; Cevallos-Urena *et al.*, 2023; Chegini *et al.*, 2020). Chitosan has an anti-biofilm effect because of the functional amino groups of N-acetylglucosamine units. The positive charge of chitosan reacts electrostatically with the negatively charged biofilm components such as EPS, DNA, and proteins, resulting in bacterial biofilm inhibitory action (Aguayo *et al.*, 2020). Several studies suggest that using bacteriophage in combination with chitosan could improve their effectiveness. Abdelsattar *et al.*, 2023 conducted a similar investigation and discovered that chitosan and bacteriophage have additive inhibitory effects on Gram-positive and Gram-negative bacteria and the formation of biofilms (Abdelsattar *et al.*, 2023). According to Adnan *et al*., 2020 findings, treatment with MA-1 phage for six hours resulted in a significant eradication (99.9%) of 74-hour-old biofilms when compared to the control group (Adnan *et al.*, 2020).

5.5.3 Microscopy of biofilm

Microscopic examination of biofilms allows a better understanding of the spatial arrangement within the biofilms and their supporting surfaces. The morphology of the biofilms was observed by the SEM **(Fig 5.13)**.

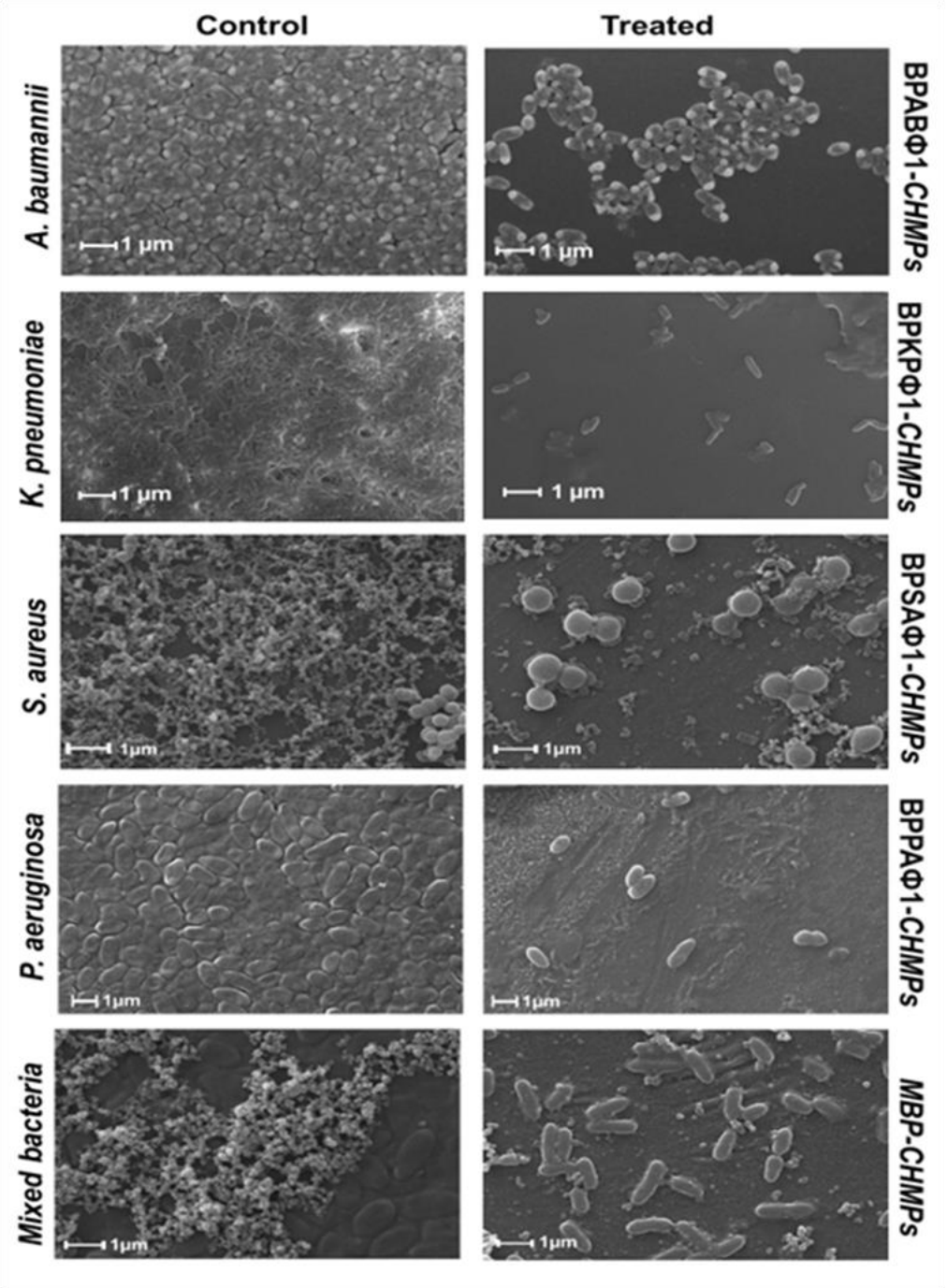

Figure 5.13 Scanning electron microscopy of biofilm consists of control biofilm of different bacteria grown on a glass coverslip and bacteriophage-treated groups which shows eradication of biofilms

The analysis using SEM revealed that the control biofilms of *A. baumannii, K. pneumoniae, S. aureus, P. aeruginosa, mixed biofilm* (*S. aureus* and *P. aeruginosa*) (**Fig. 5.13**) exhibited intricate dense arrangements of bacterial cell clusters, which were embedded within a matrix consisting of extracellular biological substances Nevertheless, upon the use of microparticles treatment, there is a notable reduction in the size, density, and removal of EPS matrix of the developed biofilm. In a recent study, the researchers investigated the combined impact of phage phiIPLA-RODI and the phage-derived lytic protein CHAPSH3b on robust biofilm formation by *S. aureus*15981 and *S. aureus* V329 strains (Duarte *et al.*, 2021).

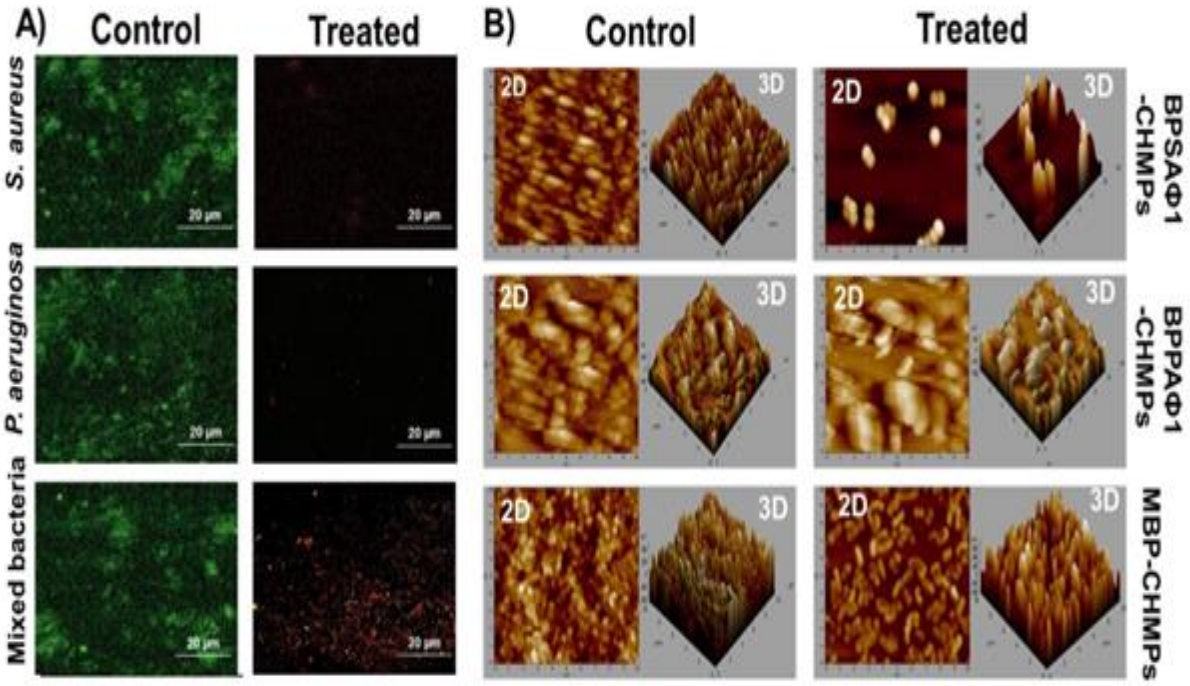

Figure 5.14 Microscopy of biofilm A) confocal laser scanning microscopy of biofilm stained by syto 9 and propidium iodide dye B) 3D complexation of mixed bacterial biofilm studied by atomic force microscopy.

Additionally, the effect of mixed bacteriophage microparticles on poly bacterial biofilm was confirmed by CLSM and AFM. CLSM (Live/dead staining) images show thick live bacteria green structures in control groups (untreated) of *S. aureus* **(Fig 5.14A, first**

row), *P. aeruginosa* **(Fig.5.14 B, second row),** and a combination of these two bacteria **(Fig.5.14C, third row).**

Treatment with BPSAΦ1-CHMPs, BPPAΦ1-CHMPs, and MBP-CHMPs depicted dead bacteria in red color with reduced biofilm thickness. Furthermore, the AFM showed a thicker biofilm spatial arrangement in comparison with a single bacterial biofilm. The result suggested that MBP-CHMPs were effective against the mixed poly bacterial biofilm. Biofilms typically demonstrate a greater proportion of persisters cells as compared to planktonic populations, thereby enhancing their capacity to endure antimicrobial challenges (de la Fuente-Núñez *et al.,* 2013). The researchers conducted a visual examination of the 24-hour-old biofilms using CLSM. They observed that the combination treatment resulted in the greatest degree of bacterial cell death. Furthermore, a plethora of research studies have been conducted to demonstrate the advantages of utilizing SEM, CLSM, and AFM for the visual examination and eradication of their intricate structures (Ansari *et al.,* 2014; Chatterjee *et al.*, 2014; de la Fuente-Núñez *et al.*, 2013; Donelli *et al.*, 2014; Powell *et al.*, 2018).

5.6 *In vivo* wound healing study

The evaluation of burn wound healing relies on measuring the degree of decrease in both the surface area and depth after the application of specific bacteriophage therapy against specific bacteria.

5.6.1 Wound healing studies on infection caused by *A. baumannii*

The evaluation of burn wound healing depends on how much area and depth are reduced following the treatment. From the study, it was observed that a higher percentage of wound closure (94.45±2.52%) was observed with BPABΦ1-CHMPs-gel (Group-3) (Fig 5.15A) as compared to the marketed formulations (Group 2:

79.21±2.65%) on the 28th day. However, the control group exhibited only 26±1.03% of wound contraction with increased pus formation, leading to increased wound area due to profuse infections **(Fig. 5.15).** Further, the histological HE-stained images of sacrificed rat skin (Fig.**5.15B**) confirmed the faster and intact re-epithelialization of the BPABΦ1-CHMPs-gel as compared to the marketed formulation. On the contrary, untreated animals do not exhibit complete re-epithelialization even on day 28.

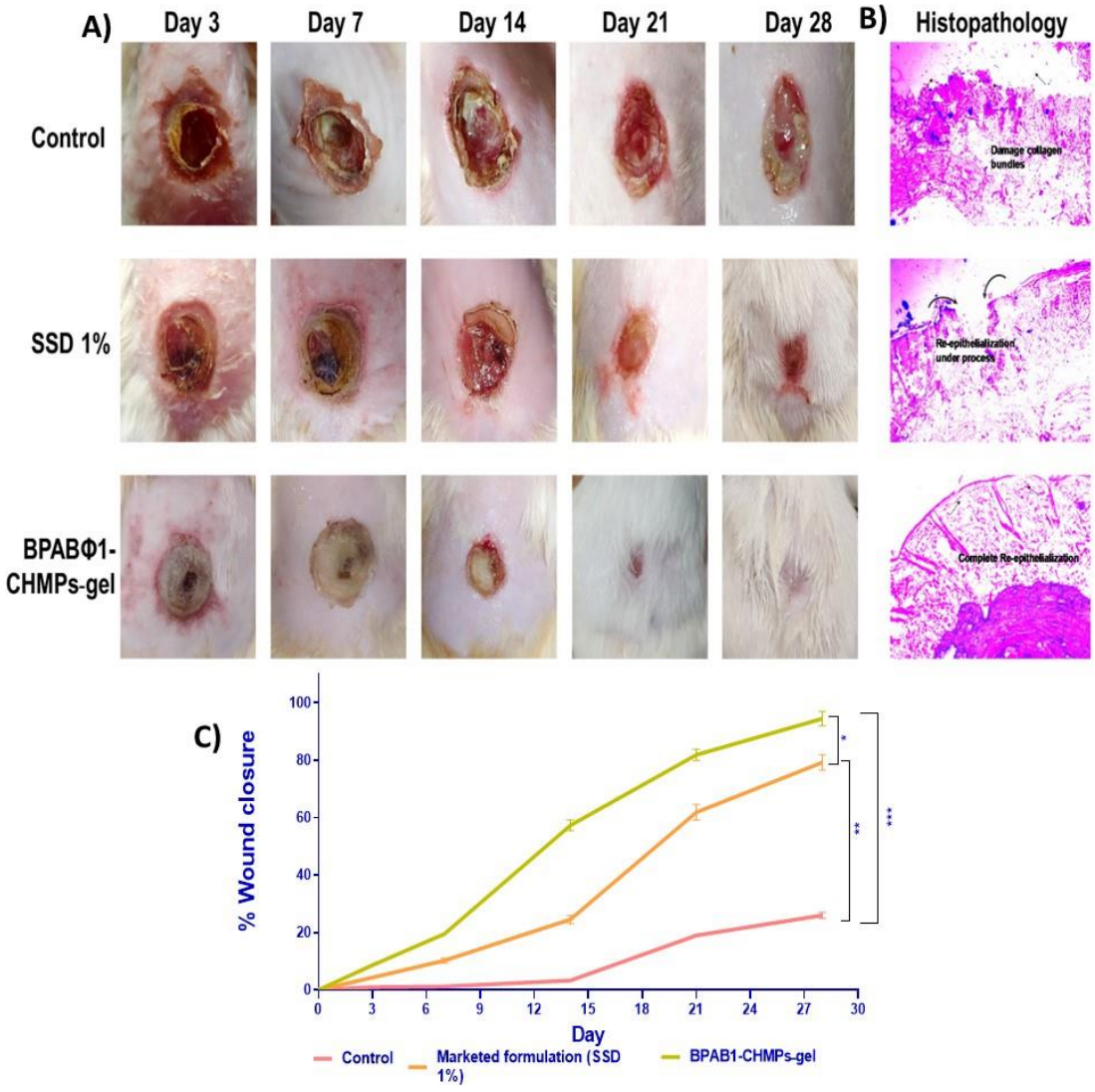

Figure 5.15 *In vivo A. baumannii* infected wound healing study on rat model where A) shows wound status on days 3, 7, 14, 21, and 28, (B) Histopathology examination of the skin of respected group, and (C) graphical data representation of % wound closure. The statistical analyses were performed by using One-way ANOVA followed by the Tukey test. * represents p < 0.001, ** represents p < 0.01 and * represents p < 0.05**

Further, the 3D-Mode of Ultrasound (USD) was employed to collect the area (two-dimensional data) and depth-volume (three-dimensional data) of the wound.

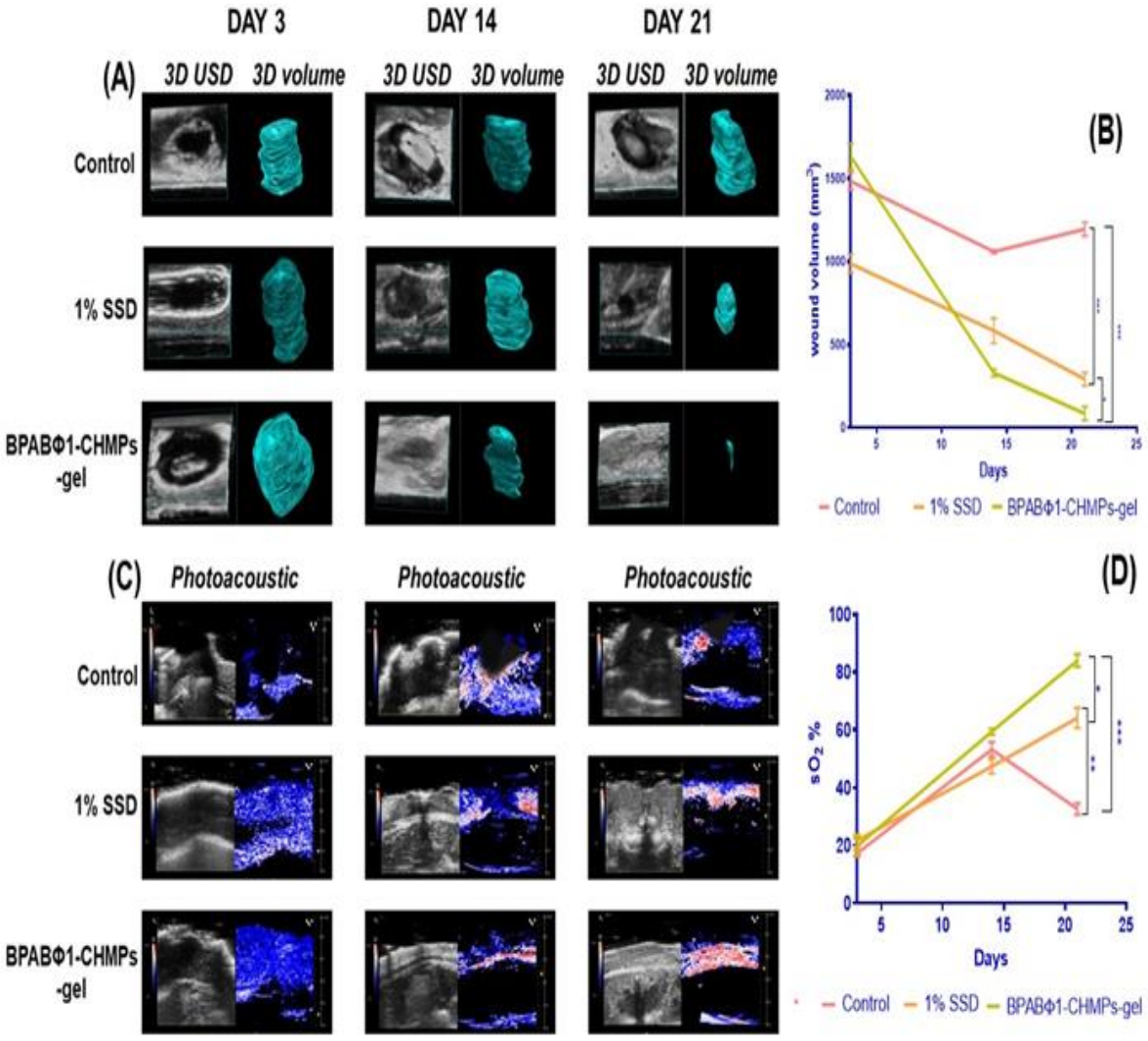

Figure 5.16 Ultrasound imaging of wound, where (A) 3D ultrasound imaging of the Control group, 1% SSD (Marketed formulation) and treatment with BPABΦ-CHMPs-gel, B) Line graph indicating the change in wound 3D volume on the Y axis and time on X axis, (C) Photoacoustic imaging of wound with (D) graphical representation of changes in sO2 % of different groups on day 3, 14 and 21. The statistical analyses were performed by using One-way ANOVA followed by the Tukey test. * represents p < 0.001, ** represents p < 0.01 and * represents p < 0.05**

USD identified the wound location and evaluated the volume (mm^3) of the wound on days 3, 14, and 21 by processing the image by multislice method from the upper surface to the underlying layer **(Fig. 5.16A)** and quantitative wound volume changes were plotted, as shown in **Fig. 5.16B**. On day 3, the wound volume was found to be

1482.81±52.12, 986.71±56.13, and 1632.29±80.99 mm^3 when treated with control (Group-1), 1% SSD (Group 2), and BPKPΦ1-CHMPs-gel (Group-3), respectively.

It was further observed that the wound volume gets reduced by treatment with BPKPΦ1-CHMPs-gel (85.12±14.24 mm^3) on day 21, although the smaller wound images were not visible in the 3D-USD images. However, it can be recognized in the 2D-USD and wound volume. Furthermore, the reduction in wound volume in 1% SSD (292.47±39.54 mm^3) was less than the prepared formulation, and the control group showed a significantly lesser decrease in wound volume (1195.42±42.23 mm^3) due to severe infection. Photoacoustic imaging (PA-Mode) was used to determine saturated oxygen percentage ($_sO_2$%). PA imaging **(Fig.5.16C)** is ideally suited to monitor local angiogenesis, perfusion, and oxygen saturation, which are the key parameters for wound healing. The day 3 oxygen saturation (sO2%) of control, 1% SSD, and BPKPΦ1-CHMPs-gel, was found (**Fig. 5.16D**) 16.91±1.12, 21.74±2.00, and 21.02±2.29%, respectively. sO2% gradually increased with increasing the day of treatment, and it was found higher in the formulation group BPKPΦ1-CHMPs-gel (84.51±2.24%) as compared to the marketed formulation (64.16±3.54%). But in the control group, the sO2% increased (53.24±2.72%) till day 14, which decreased (32.33±1.14%) on day 21 due to serious infection.

5.6.2 Wound healing studies on infection caused by *K. pneumoniae*

The evaluation of burn wound healing depends on how much area and depth got reduced upon the application of the formulation (treatment). The study **(Fig. 5.17)** findings revealed that BPKPΦ1-CHMPs gel (Group-3) exhibited a significantly higher wound closure rate (89.21±2.02%) compared to the marketed formulations (Group 2: 72.07±1.76%) on the 28th day **(Fig 5.17C).**

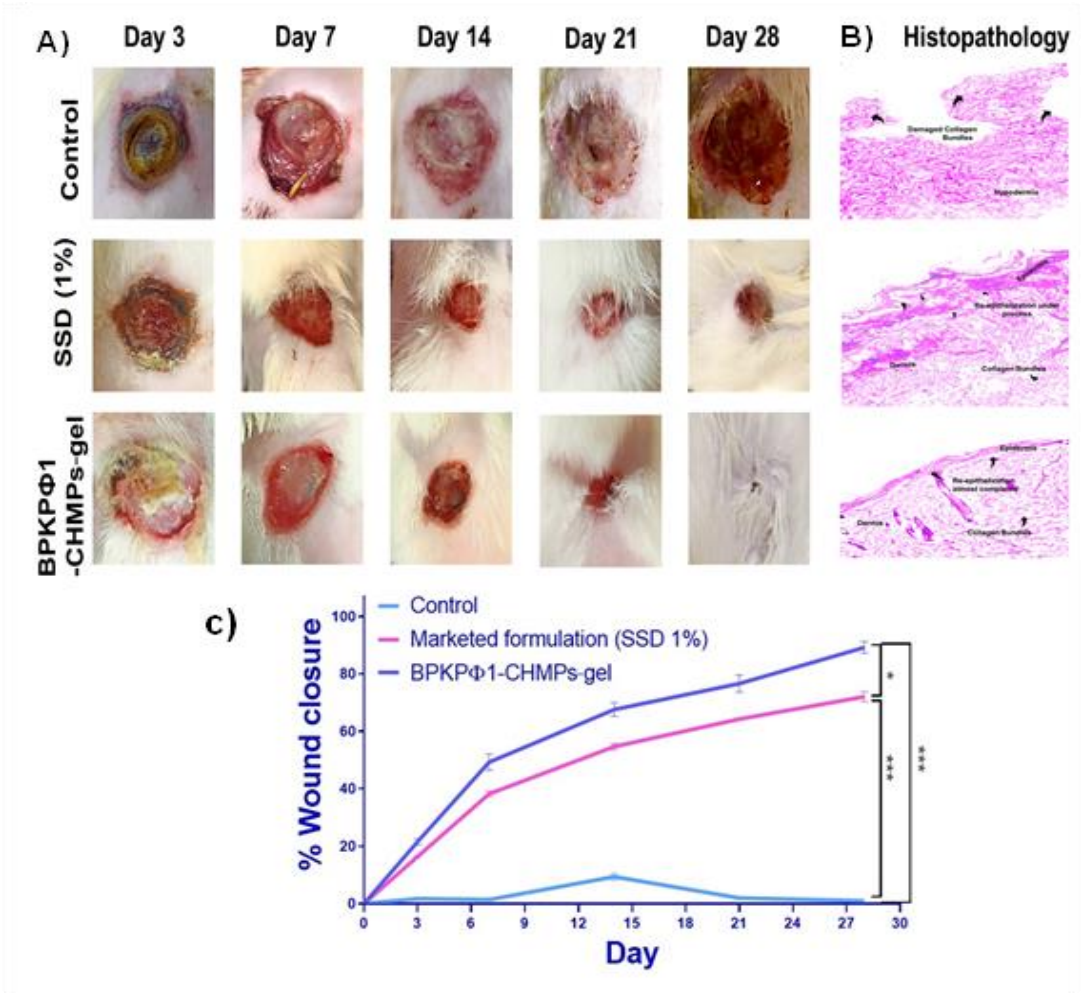

Figure 5.17 *In vivo* wound healing study where, (A) shows wound status on different days 3, 7, 14, 21, and 28, (B) histopathology examination of the skin, and (C) graphical representation of % wound closure. The statistical analyses were performed by using One-way ANOVA followed by the Tukey test. * represents p < 0.001, ** represents p < 0.01 and * represents p < 0.05**

The utilization of a three-dimensional (3D) mode of ultrasound (USD) imaging was used to acquire both the two-dimensional data of the wound area and the three-dimensional data of the depth-volume. USD imaging analyzed the wound volume on days 3,14, and 21 by processing the image using a multislice method from the top layer to the bottom layer **(Fig. 18A–C).** Quantitative changes in wound volume were plotted in **Fig. 5.18D.** On the third day of observation, the wound volumes were measured to be 537.26±25.04, 719.00±19.24, and 702.14±18.44 mm^3 for the control group (Group-1), the 1% silver sulfadiazine (SSD) group (Group-2), and the BPKPΦ1-CHMPs-gel group

(Group-3) respectively. The study also revealed that the application of BPKPΦ1-CHMPs-gel resulted in a decrease in wound volume (83.161±9.77 mm^3) on day 21.

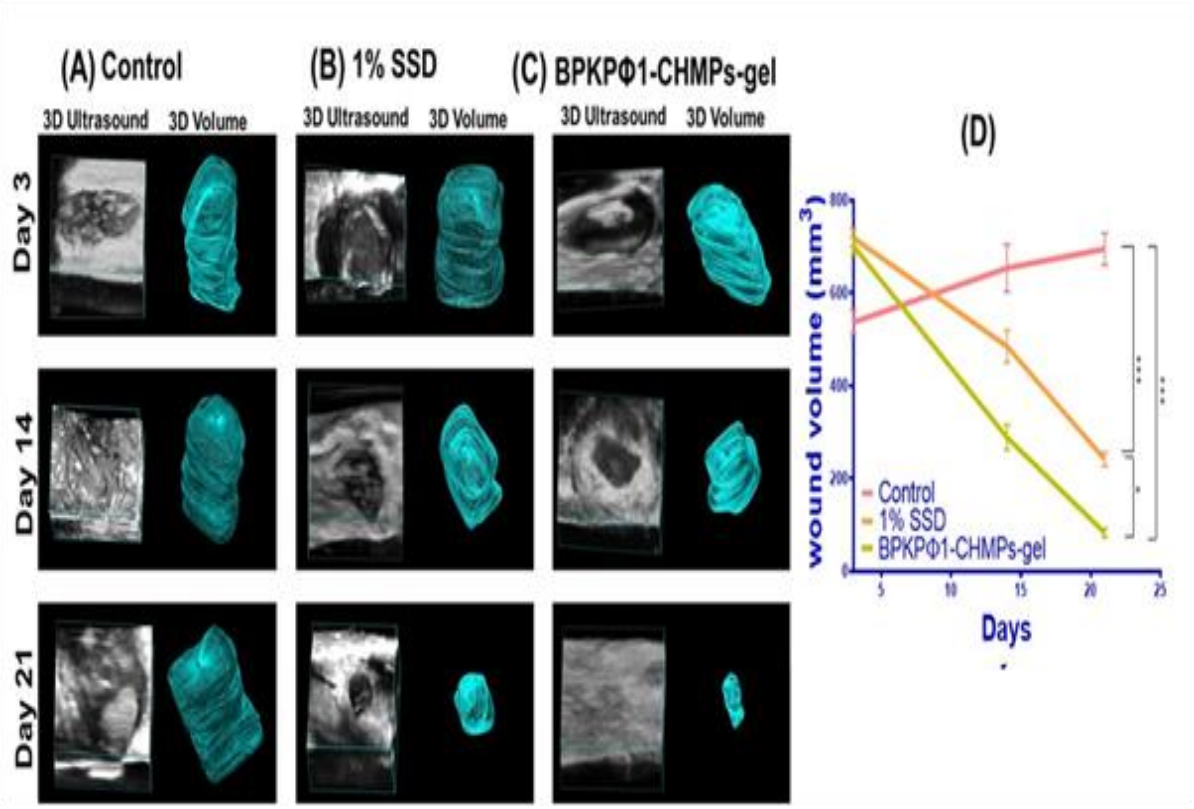

Figure 5.18 Ultrasound imaging of wound, where A) Control group, B) 1% SSD (Marketed formulation), C) treatment with BPKPΦ-CHMPs-gel, and D) Line graph indicating the change in wound volume on the Y axis and time on X axis. The statistical analyses were performed by using One-way ANOVA followed by the Tukey test. * represents p < 0.001, ** represents p < 0.01 and * represents p < 0.05**

Although the smaller wound images were not distinctly visible in the 3D-USD images **(Fig. 5.18C- Day 21 BPKPΦ-1-CHMPs-gel**), they could be identified through the 2D-USD and wound volume measurements. In addition, it is worth noting that the decrease in wound volume observed in the group treated with 1% SSD (241.85±15.11 mm^3) was somewhat lesser than that observed in the group treated with the bacteriophage formulation. Conversely, the control group exhibited an increase in wound volume (695.24±34.09 mm^3) as a result of a chronic infection.

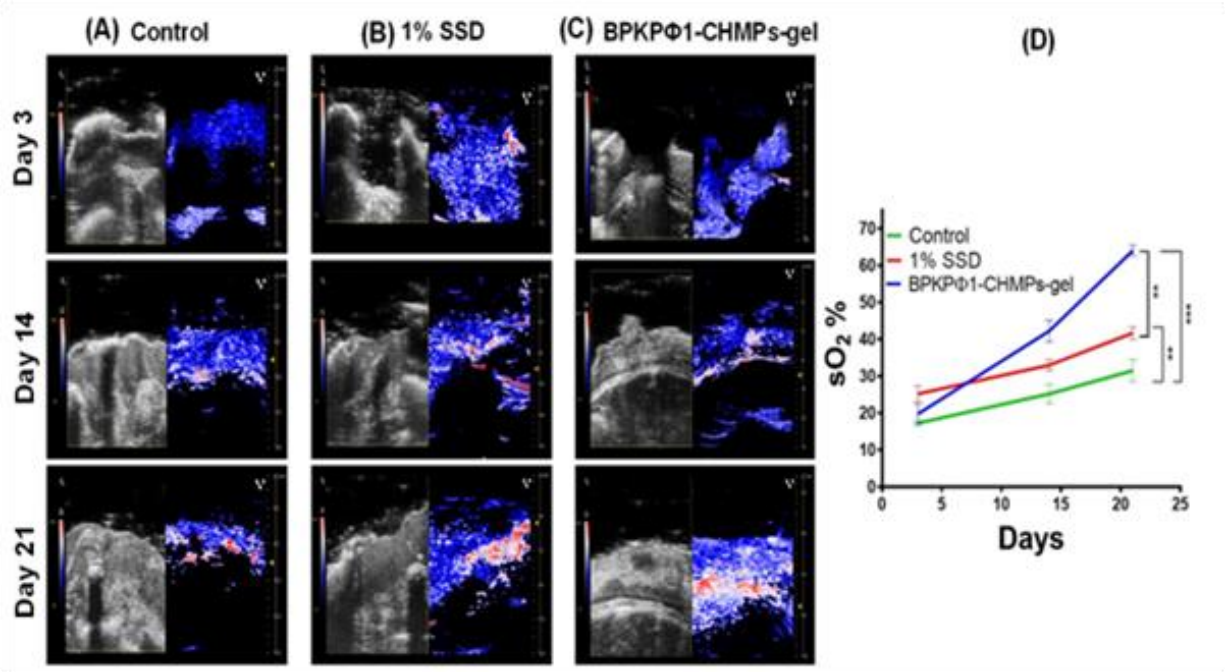

Figure 5.19 Photoacoustic analysis of wound infection caused by *K. pneumoniae* bacteria where, (A) Control group, (B) 1% SSD (Marketed formulation), and (C) treatment with BPKPΦ-1-CHMPs-gel and, (D) line graph representing the sO2% on the Y axis and time on X axis. The statistical analyses were performed by using the One-way ANOVA followed by the Tukey test. * represents p < 0.001, ** represents p < 0.01 and * represents p < 0.05.**

Photoacoustic imaging (PA-Mode) was used to determine saturated oxygen percentage ($_sO_2$%). PA imaging **(Fig. 5.19)** is ideally suited to monitor local angiogenesis, perfusion, and oxygen saturation, which are the key parameters for wound healing. The day 3 oxygen saturation (sO2%) of control, 1% SSD, and BPKPΦ1-CHMPs-gel, was found **(Fig. 5.19D)** 17.22±0.69, 25.18±1.54, and 19.77±2.1%. sO2% gradually increased with increasing the day of treatment, and it was found higher in formulation group BPKPΦ1-CHMPs-gel (64.05±1.45%) as compared to marketed formulation (47.70±2.37%) and control group (31.51±1.49%) on day 21.

5.6.3 Wound healing studies on infection caused by poly bacterial strains

The evaluation of burn wound healing is a crucial aspect of assessing the progress and effectiveness of burn wound treatment. It involves a comprehensive assessment of two primary factors: the area of the burn and the depth of the burn.

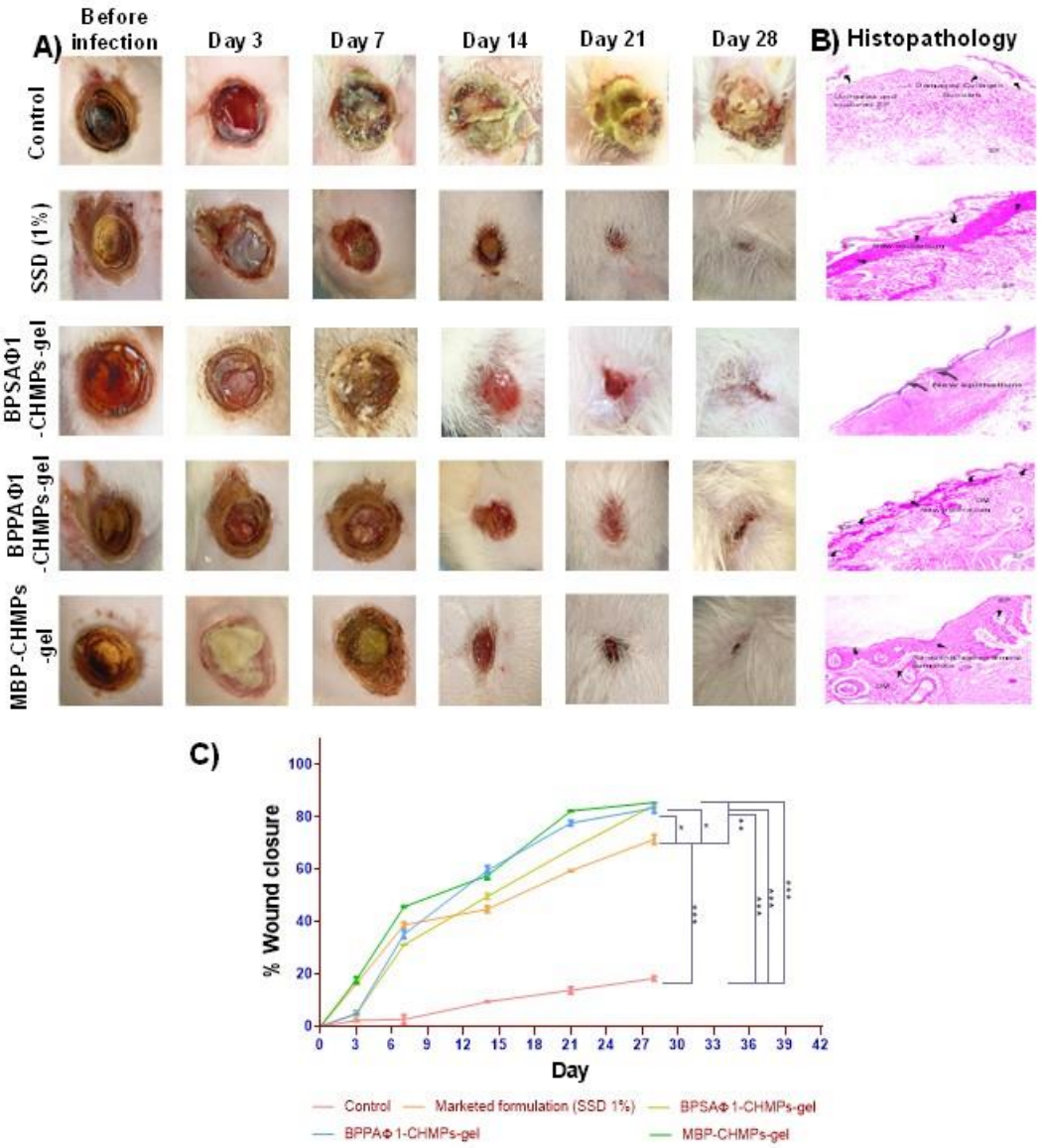

Figure 5.20 Burn wound healing assay against wound infections caused by single bacterial (*S. aureus or P. aeruginosa*) and poly bacterial strains where, A) Effect of BP formulations in burn wound on different days, B) histopathology examination at the end of the healing where arrow mark shows damaged collagen bundles with ruptured epithelium in the control group and formation of new epithelium membrane in other groups. C) The graph depicts the percentage of wound closure with time (days). The statistical analyses were performed by using the One-way ANOVA followed by the Tukey test. * represents p < 0.001, ** represents p < 0.01 and * represents p < 0.05**

The percentage of wound closure **(Fig. 5.20)** after treatment with BPSAΦ1-CHMPs-gel (Group-III), BPPAΦ1-CHMPs-gel (Group-IV), and MBP-CHMPs-gel (Group-V) were found to be 84.61±1.03, 83.38±1.87, and 85.54±0.05% on 28th day, whereas marketed formulation (Group-II) treated animals had 71.47±1.75% of wound closure. The control group also showed around 18% wound contraction however, pus formation was also

noticed with time. Moreover, the results confirmed the effectiveness of BPs combination in the treatment of poly-bacterial infections.

Furthermore, the histological HE-stained images of sacrificed rat skin **(Fig. 5.20B)** confirmed the faster and intact re-epithelialization of the BPSAΦ1-CHMPs-gel, BPPAΦ1-CHMPs-gel, MBP-CHMPs-gel treatment group in comparison with the marketed formulation. On the contrary, untreated animals **(Fig. 5.20B)** did not have complete re-epithelialization on day 28. Similar observations were reported in previous reports by different groups. For instance, lytic phases φAB140 and φAB150 chitosan formulation showed a significant decrease in wound size caused by MDR bacterial infection (Ilomuanya *et al.*, 2022). In a recent study conducted by Rezk *et al.*, 2022, it was discovered that phage ZCPA1 exhibits an effective antibacterial efficacy against multidrug-resistant *P. aeruginosa*. The study further demonstrated that the application of phage ZCPA1 resulted in significant improvements (99.84%) in wound healing effects in a rat model with full-thickness infection of a wound (Rezk *et al.*, 2022). Antibiotic ineffectiveness in antimicrobial-resistant wound infections imposes an immense medical and financial burden, highlighting the need for new treatments to remove obstacles to wound healing in wound care.

A 3D-Mode of Ultrasound (USD) was used for collecting two-dimensional (area) and three-dimensional (depth and volume) data on the wound. PA-Mode was used for determining saturated oxygen percentage (SO_2%). USD identified the wound location and evaluated the volume (mm^3) of the wound on days 3, 14, and 21, processing the image by the multislice method from the upper surface to the underlying layer **(Fig 5.21),** and quantitative wound volume changes were plotted**.** On day 3, the wound volumes of control (Group-I), 1% SSD (Group-II), BPSAΦ1-CHMPs-gel (Group-III), BPPAΦ1-CHMPs-gel (Group-IV), and MBP-CHMPs-gel (Group-V) was found to be

481.40±12.12, 444.68±16.0, 469.276±27.9, 442.25±25.14, and 425.23±23.12 mm^3, respectively.

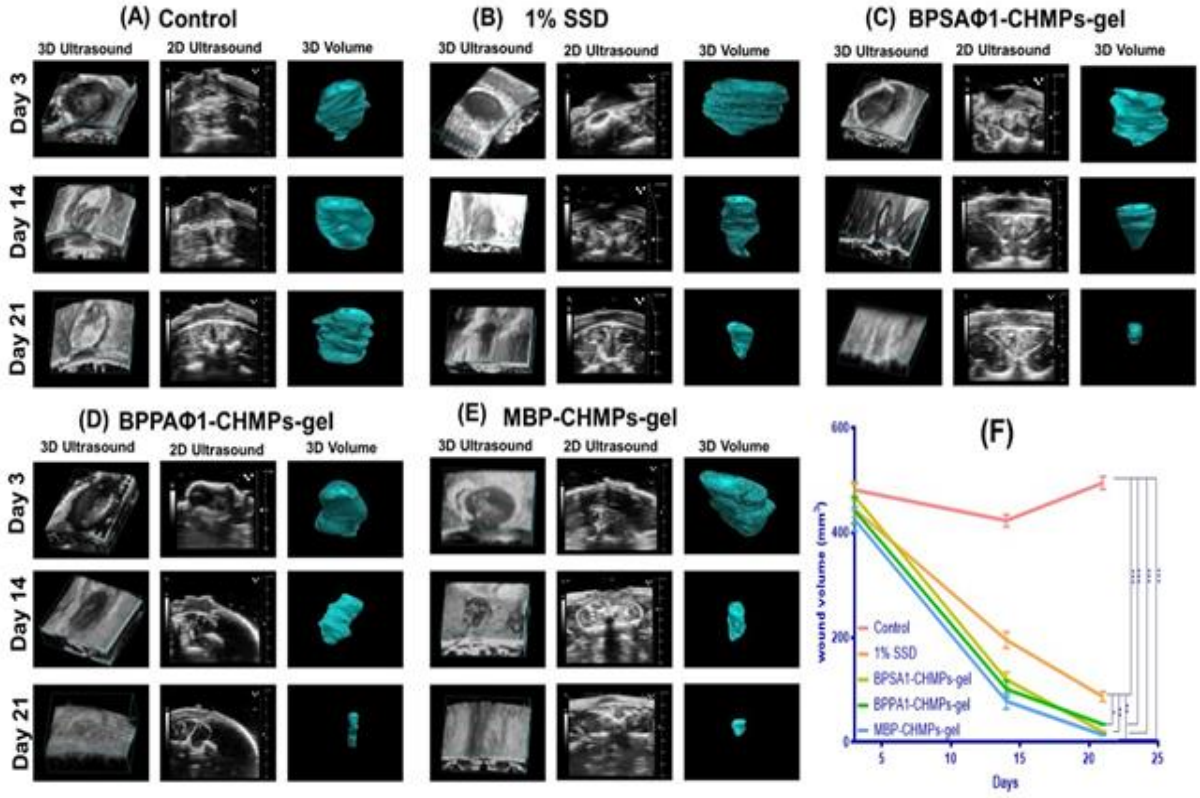

Figure 5.21 Ultrasound imaging of infected burn wound where (A) represents the control group (without treatment), (B) treated with 1% SSD (marketed formulation), (C) treated with BPSAΦ1-CHMPs-gel, (D) treated with BPPAΦ1-CHMPs-gel and (E) treated with MBP-CHMPs-gel. F) graphical representation of quantitative measurement of wound volume on different days. The statistical analyses were performed by using the One-way ANOVA followed by the Tukey test. * represents p < 0.001, ** represents p < 0.01 and * represents p < 0.05**

The volumes of the wound after treatment with BPSAΦ1-CHMPs-gel (20.161±1.24 mm^3), BPPAΦ1-CHMPs-gel (34.60±0.92 mm^3), and MBP-CHMPs-gel (14.16±1.400 mm^3) were reduced significantly in day 21. Although the smaller wound images were not visible in the 3D-USD images **(Fig. 5.21C, 5.21D, and 5.21E)**, they can be recognized in the 2D-USD and wound volume. Furthermore, the reduction in wound volume in 1% SSD (87.027±9.54 mm^3) was less than the prepared formulation, and the control group shows a slight increase in wound volume (494.74±12.20 mm^3) **(Fig. 5.21F)** due to heavy infection. USD images clearly showed the deeper damage to the

skin layer on day 3 and as the burn wound recovered, the burn depth started to decrease gradually (day 14). Since post-burn day 21, burn depth has been gradually reduced after treatment with bacteriophage solution. Therefore, BP formulations have demonstrated efficacy in treating antibiotic-resistant bacterial wound infections caused by specific strains.

PA imaging **(Fig. 5.22)** is ideally suited to monitor local angiogenesis, perfusion, and oxygen saturation. These are all key parameters for wound healing. The day 3 oxygen saturation (sO_2%) of control, 1% SSD, BPSAΦ1-CHMPs-gel, BPPAΦ1-CHMPs-gel, and MBP-CHMPs-gel groups **(Fig. 5.22)** were found to be 24.41±1.08, 30.403±1.3, 29.824±2.33, 19.63±2.13, and 21.1±1.82 %, respectively. sO_2% gradually increased as the day of treatment progressed, and the level of sO_2% was higher in formulation-treated groups, BPSAΦ1-CHMPs-gel (81.20±0.74 %), BPPAΦ1-CHMPs-gel (75.40±0.94 %), MBP-CHMPs-gel (89.45±0.40 %) as compared to marketed formulation (69.25±0.54%) and control group (34.89±0.81 %) on day 21. Interestingly, the central area of the burn had more hypoxia compared to the surrounding area in the first week as confirmed by sO_2 images. This was mainly caused by dermal damage and a lack of blood perfusion. The sO_2% increased with increasing post-burn days due to the recovery of blood perfusion.

Existing literature highlights the relevance of USG/PA imaging as an emerging tool for analyzing wound healing. Similarly, a multiscale photoacoustic assessment was used to determine the efficacy of the chitosan-graphene oxide (CH-Go) hemostatic sponge (Lin *et al.*, 2021). After analyzing the data, they concluded that the Chi-GO hemostatic sponge showed promising results in terms of hemostatic application, wound therapy, and targeted medication release.

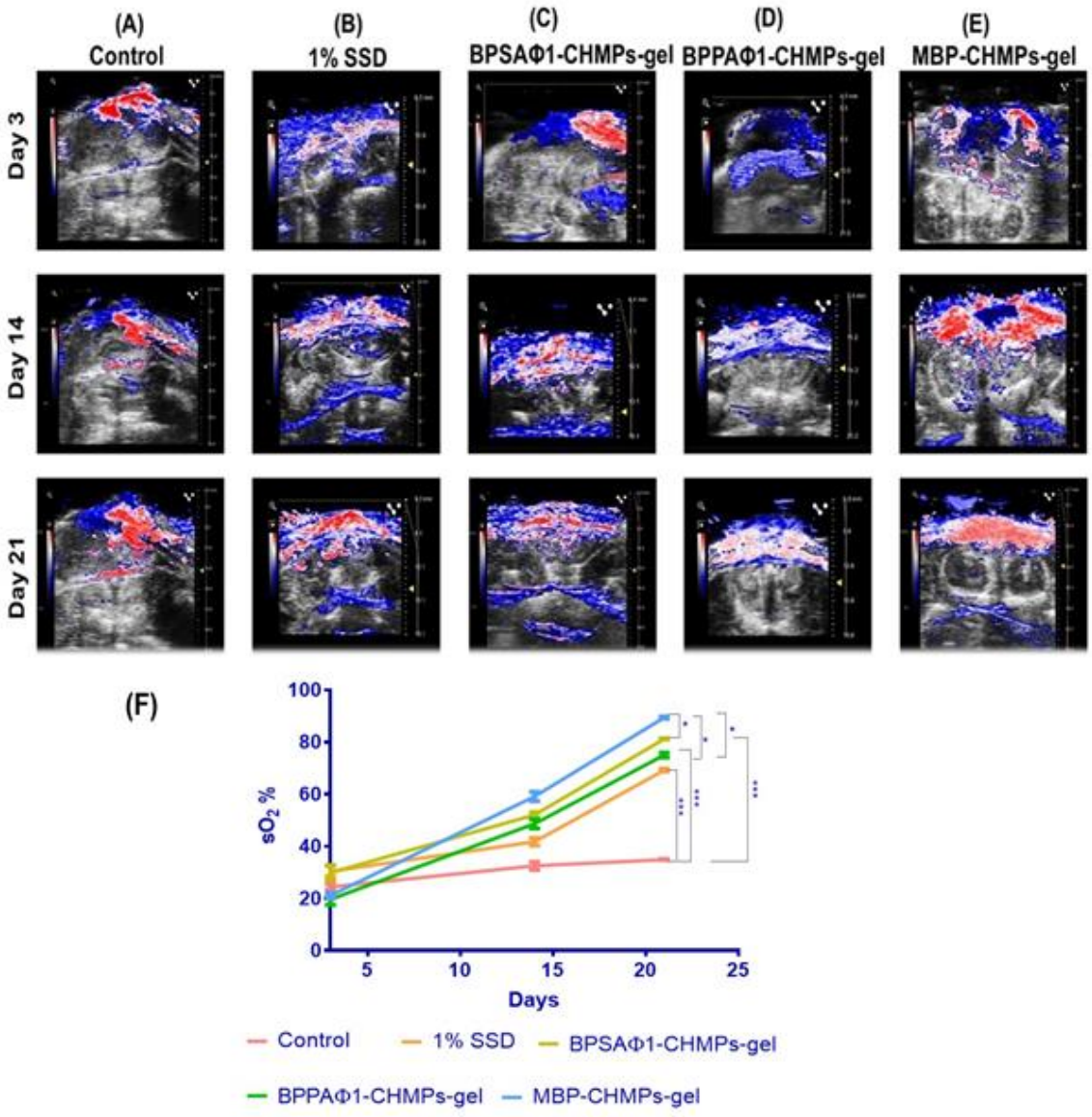

Figure 5.22 Ultrasound and Photoacoustic imaging of infected wound where, (A) Control group (without treatment), (B) treated with 1% SSD (marketed formulation), (C) treated with BPSAΦ1-CHMPs-gel (D) BPPAΦ1-CHMPs-gel and (E) treated with MBP-CHMPs-gel. (F) graphical representation of quantitative oxygen saturation measurement on days 3, 14, and 21. The statistical analyses were performed by using the One-way ANOVA followed by the Tukey test. * represents $p < 0.001$ and * represents $p < 0.05$**

Mantri *et al.*, 2022 evaluated the use of PA-US to track angiogenesis in 19 clinical patients. In this study, local angiogenesis, tissue perfusion, and oxygen saturation were studied for 3 weeks along with 3Dmap wound bed physiology. They concluded that PA imaging is the most effective method for predicting wound healing. This imaging may help clinicians decide whether to start, continue, adjust, or stop therapy earlier (Mantri

et al., 2022). Usually, clinicians assess wound health based on surface indications such as color, odor, skin texture, discharge, edema, and the presence of weakened tissue. USH/PA imaging can be used to measure wound area, wound volume, angiogenesis rate, and formation of scar tissue.

5.7 Gel occlusion and bioimaging study

In this study, DiD dye (fluorescent dye) was used as a model dye for fluorescent imaging. DiD dye-loaded MPs and microparticles-laden gel were evaluated for sustained fluorescent signal and correlating with BP release or sustained activity on the wound site **(Fig. 23).** From fluorescent imaging **(Fig. 23A),** it was observed that DiD-CHMPs and DiD-CHMPs-gel both are site-specific and not distributed to other body organs when evaluated up to 12 h at the interval of 3 h. Moreover, DiD-CHMPs-gel was not only easy to apply but also remained on the wound site (fluorescent intensity 3.69e7±100250 – 1.27e6±45900) for more than 12 h without any significant loss of fluorescent intensity. However, DiD-CHMPs formulation after its application shows a gradual decrease in the fluorescent intensity with time, more significantly compared to the microparticle loaded gel **(Fig. 23B).** On the contrary, DiD-CHMPs was a little inconvenient to apply, retain only in a corner portion of wound and came off in 8 h with faster decrease in fluorescent intensity from 2.65e7±98600 to 3.2e2±80. Hence, from the obtained results, the conclusion can be drawn that the gel formulation exhibited a longer retention time of 12 h compared to the commonly used BP solution. This extended retention can be attributed to the formation of a gel layer around the skin when the gel is applied.

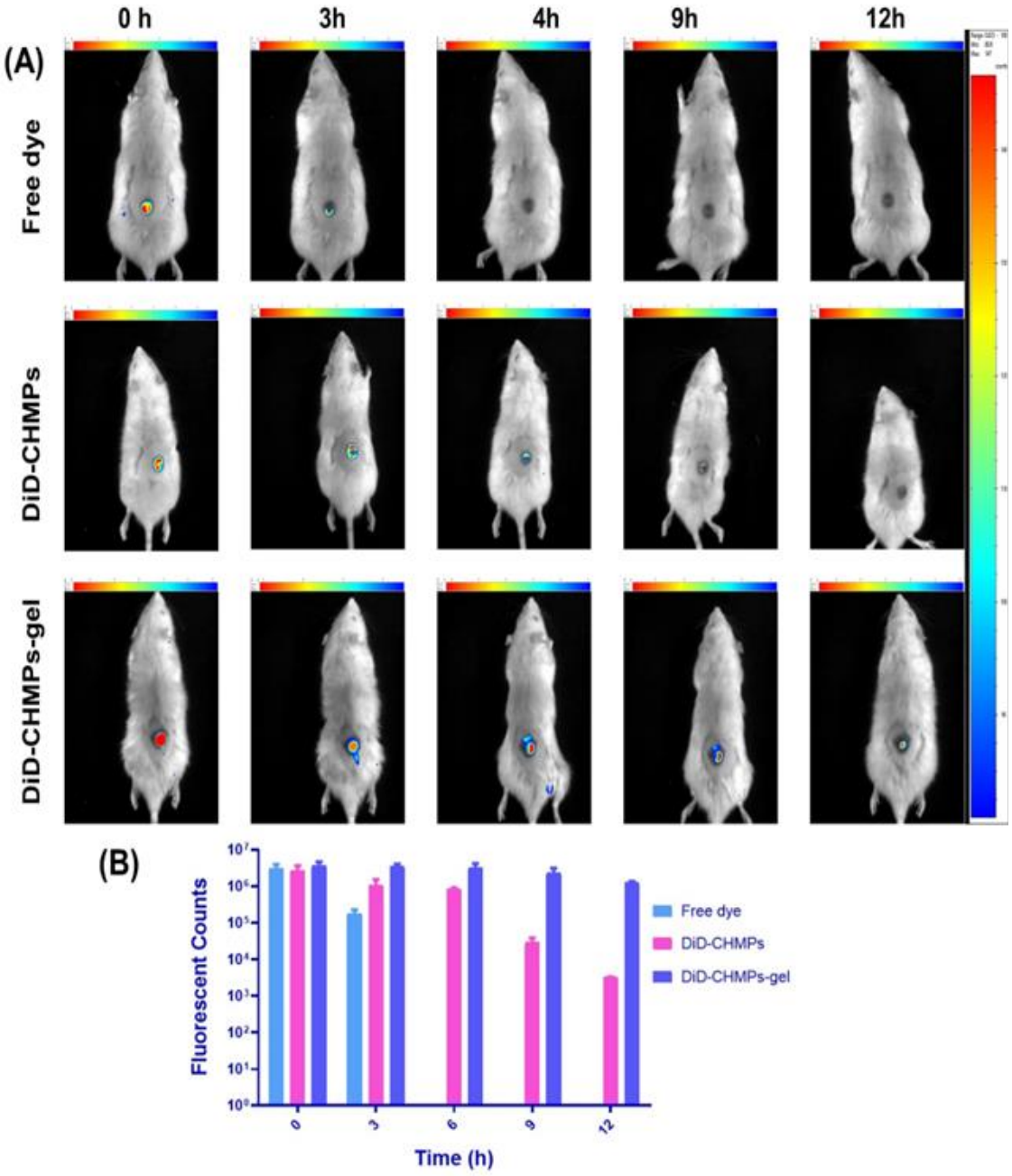

Figure 5.23 (A) *In vivo* fluorescence imaging and gel occlusion study for 12 h after application of the free DiD, DiD-CHMPs and DiD-CHMPs-gel on rats' wounds. (B) Graphical representation of fluorescence intensity of free DiD, DiD-CHMPs, and DiD CHMPs-gel after application to the wound at different time intervals

Puthia *et al.*, 2020 used *in vivo* bioimaging to evaluate the efficiency of a TCP-25 peptide-functionalized hydrogel in treating *S. aureus* and *P. aeruginosa*-infected partial-thickness wounds. They examined the TCP-25 biodistribution in vivo after injecting SKH1 mice dorsum with TCP-25 gel that has been Cy5-labeled. The diffusion of the peptide from the gel into the surrounding tissues was tracked using longitudinal IVIS

bioimaging. The findings indicated that TCP-25 exhibited significant retention at the site of injection (Puthia *et al.*, 2020).

5.8 Stability studies

The stability study found that BPABΦ1 suspension was found to be unstable (**Fig 5.24 A**), as it showed ~80% decreased titer within a month at a temperature of 4.0 ± 0.2 °C, with minimal antibacterial activity within 3 months. However, the entrapped bacteriophage titer in the cases of BPABΦ1-CHMPs and BPABΦ1-CHMPs gel (Figure 3) first declined (first month) by one-tenth titer, but after that, it remained stable for up to three months at 4.0 ± 0.2 °C. This stability could be due to the protective nature of trehalose and glycerin in the developed formulation.

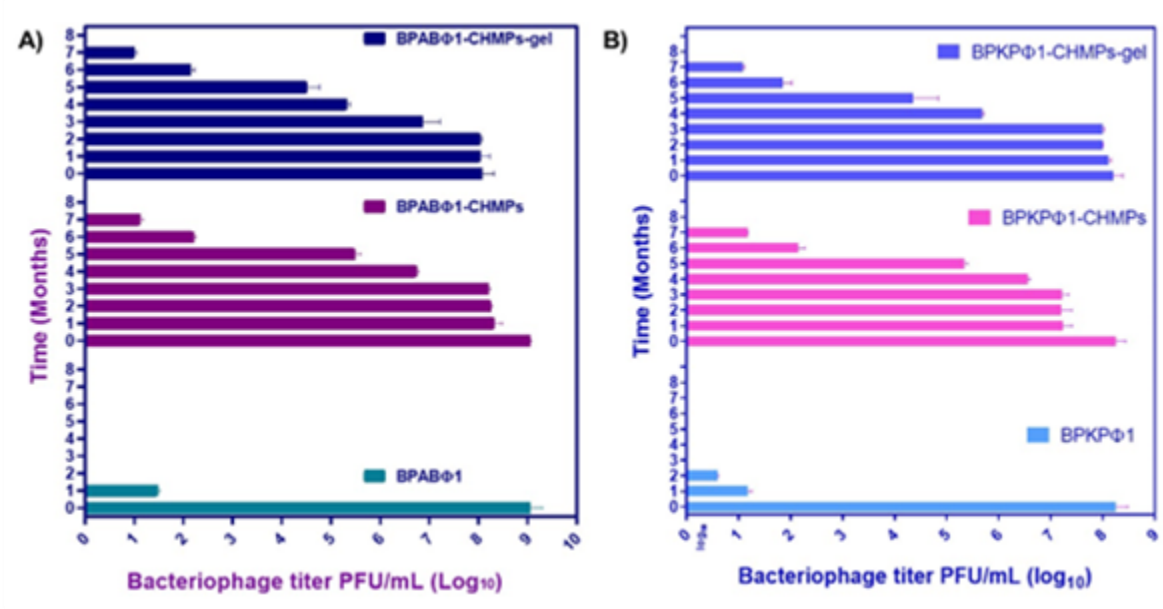

Figure 5.24 Stability studies where graphs represent the bacteriophage titer with respect to time. A) Isolated bacteriophage BPABΦ1 suspension, and prepared formulations BPABΦ1-CHMPs, and BPABΦ1-CHMPs-gel B) Isolated bacteriophage BPKPΦ1 suspension, BPKPΦ1-CHMPs, and BPKPΦ1-CHMPs-gel

In the case of pure BPKPΦ1 solution was found to be unstable **(Fig. 5.24B),** as it showed more than half titer decreased within a month at a temperature of 4.0±0.2°C, with a complete loss of antibacterial activity within 1 month. However, in the case of BPKPΦ1-CHMPs and BPKPΦ1-CHMPs-gel **(Fig 5.24B)**, the titer get decreased by

one-tenth in the first month and later it was maintained for up to 4 months at 4.0±0.2℃ and this stability could be assigned to the protective nature of trehalose and glycerine present in the developed formulation.

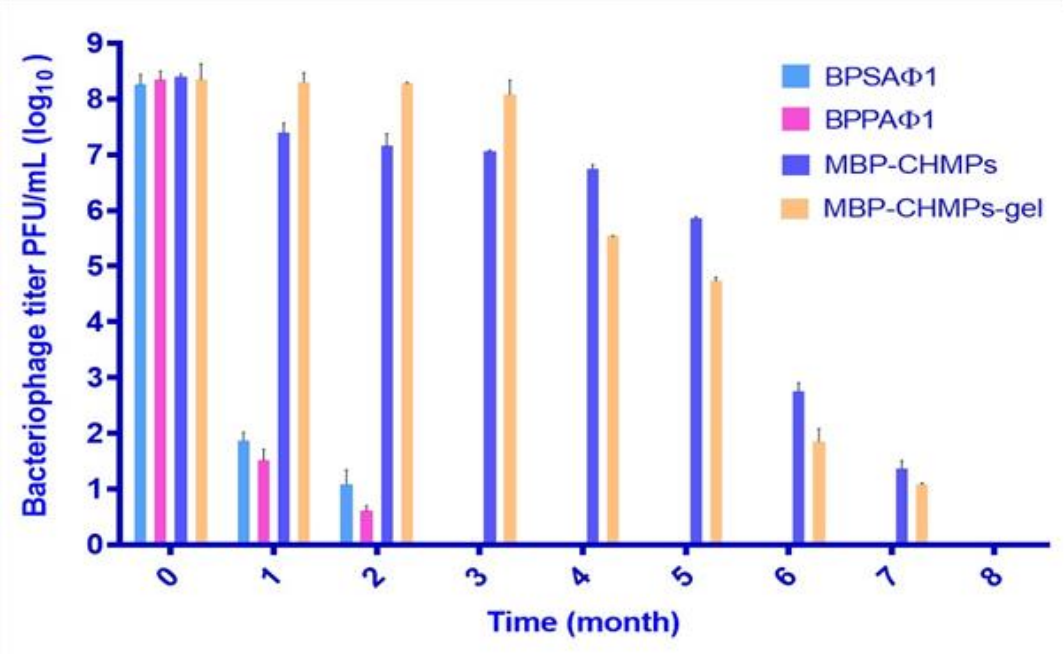

Figure 5.25 Stability studies of the BPSAΦ1 and BPPAΦ1 bacteriophage suspensions and their microparticle and gel formulations

The stability study **(Fig. 5.25)** results indicated that the pure BP solutions were found unstable due to the decrease in more than 50% of BPs titer within a month at 4.0±0.2℃, while a complete loss of activity was observed in 3 months. In the case of MBP-CHMPs and MBP-CHMPs-gels, the titer decreased by one-tenth in the first month. However, it was maintained for up to 4 months when stored at 4.0±0.2℃, and this stability could be attributed to the protective nature of trehalose and glycerine present in the developed formulation. Several reports have suggested that the addition of trehalose enhances the stability of bacteriophages (Brogna *et al.*, 2020; Petsong *et al.*, 2021; Wdowiak *et al.*, 2022). The results demonstrated that trehalose exhibited a decrease in the accumulation of reactive oxygen species and protein oxidation products throughout storage. Trehalose-based bacteriophage antimicrobial films/coatings exhibit significant promise in the extended preservation of bacteriophages (Leung *et al.*, 2018).